MASTER

Atomic Energy of Canada Limited

METHODS FOR NEUTRON SPECTROMETRY

CRNP-947

by

B.N. BROCKHOUSE

Chalk River, Ontario

January 9, 1961

AECL-1183

DISCLAIMER

Portions of this document may be illegible in electronic image products. Images are produced from the best available original document.

ATOMIC ENERGY OF CANADA LIMITED
Research and Development

METHODS FOR NEUTRON SPECTROMETRY

CRNP 947

by
B.N. Brockhouse

This paper was presented as Paper No. IS/18 at the Symposium on Inelastic Scattering in Solids and Liquids, Vienna, October 11-14, 1960.

Chalk River, Ontario
January 9, 1961

AECL 1183

METHODS FOR NEUTRON SPECTROMETRY

B.N. Brockhouse

Atomic Energy of Canada Limited

Chalk River, Ontario, Canada

A B S T R A C T

Measurements of the energy distributions of initially monoenergetic neutrons after scattering by a specimen, give a great deal of information about the structural dynamics of the specimen material on an atomic scale. The power of the method lies primarily in the circumstance that the energy and momentum distributions of the scattered neutrons reflect a rather complete description of the characteristic energies and momenta of the specimen material. Thus it is usually possible to obtain information directly about the dynamics of the specimen by inverting the measurements (if the set of neutron energy distributions is sufficiently complete), instead of being restricted to comparison of measured distributions with calculations based on oversimplified models. In the paper the appropriate theories, and the general philosophy of methods of measurement and of treatment of data, are discussed from the point of view of making the fullest use of the unique power of the method. In particular methods of analysis of results for liquids using the Van Hove formulation, and for crystals using the Born-von Kármán theory, are discussed at length.

In the author's opinion the most useful of the available methods of measurement are the crystal spectrometer methods and the pulsed monoenergetic beam/time-of-flight method. Pulsed-beam spectrometers have the advantage of higher counting rates than crystal

spectrometers, especially in view of the fact that simultaneous measurements in several counters at different angles of scattering are possible in pulsed-beam spectrometers. The crystal spectrometer permits several valuable new types of specialized experiments to be performed, especially energy distribution measurements at constant momentum transfer (the "constant Q" method). The Chalk River triple-axis crystal-spectrometer is described and discussed, particularly with reference to its use in making these specialized experiments. This instrument has been gradually assembled as a result of six years' experience of neutron spectrometry measurements. The Chalk River rotating crystal (pulsed-beam) spectrometer is also described and a comparison of this type of instrument with other types of pulsed beam spectrometers is made. (Several versions of this instrument have been used in the past three years.) A partial outline of the theory of operation of rotating crystal spectrometers is presented. The use of quartz crystal filters for fast neutron elimination and for order elimination is discussed.

1. INTRODUCTION AND GENERAL THEORY

The neutron has a mass of the order of atomic masses, and hence a slow neutron, in collision with a system of atoms, has a reasonable chance of picking up or losing quanta of any of the characteristic energies of the system. The wavelength of a slow neutron is of the order of atomic separations and its energy is of the order of thermal energies, that is of the order of the characteristic energies of solids or liquids. The changes in energy of the scattered neutrons are relatively large, and

easily measurable. At the same time since its wavelength is short the neutron responds to all kinds of motions in the specimen, and not just to those motions in which large numbers of atoms move together, as in the scattering of light.

The scattering is primarily governed by the energy transfer

$$\hbar\omega = E_o - E' \tag{1.1}$$

and by the wave vector transfer

$$\underset{\sim}{Q} = \underset{\sim}{k}_o - \underset{\sim}{k}' \tag{1.2}$$

where E_o and E' are the energies of the incident and scattered neutrons, and $\underset{\sim}{k}_o$ and $\underset{\sim}{k}'$ are their wave vectors. In the notation used here a subscript "O" means that the quantity concerned is evaluated at the incoming energy e.g. $\underset{\sim}{Q}_o$ is the wave vector transfer with the scattering elastic. A primed quantity has been singly scattered in the experiment, a doubly primed quantity doubly scattered, etc. The energies and wave vectors are connected by the relation $E = \hbar^2 k^2/2m_N$ where m_N is the neutron mass. Other symbols used are: the angle of scattering (ϕ), the specimen orientation in the scattering plane (ψ), the coherent scattering cross section (σ_{COH}), the incoherent scattering cross section (σ_{INC}), the mass of the atoms (M), the temperature (T), the angle of scattering by a crystal in Bragg reflection (2θ).

In fact VAN HOVE (1) has shown that, provided the temperature is high enough that there is no nuclear spin or isotope degeneracy, the partial differential cross section per atom for a monatomic system is

$$\frac{d^2\sigma}{d\Omega\, dE} = \hbar^{-1}\frac{k'}{k_0}\left\{\frac{\sigma_{COH}}{4\pi} S_{COH}(\underset{\sim}{Q},\omega) + \frac{\sigma_{INC}}{4\pi} S_{INC}(\underset{\sim}{Q},\omega)\right\} \quad (1.3)$$

Thus, in the first Born approximation, the partial differential scattering cross section is a function only of the variables $\underset{\sim}{Q}$ and ω, except for the trivial term k'/k_0. This fact provides a convenient way of coalescing the three dimensional function $\sigma(E_0,E;\phi)$ for a liquid or gas into a two dimensional function $S(Q,\omega)$ (2). For an anisotropic system, e.g. a crystal, five variables are reduced to four. Perhaps more importantly the variables $\underset{\sim}{Q}$ and ω are the wave vector and angular frequency of excitations in the specimen and are thus natural variables for the specimen also.

VAN HOVE (1) showed that the functions S are Fourier transforms of correlation functions for the atoms, which for classical systems have simple interpretations.

$$S_{INC}(\underset{\sim}{Q},\omega) = \frac{1}{2\pi}\int \exp i(\underset{\sim}{Q}\cdot\underset{\sim}{r} - \omega t)\, G_s(\underset{\sim}{r},t)\, d\underset{\sim}{r}\, dt \quad (1.4a)$$

$$S_{COH}(\underset{\sim}{Q},\omega) = \frac{1}{2\pi}\int \exp i(\underset{\sim}{Q}\cdot\underset{\sim}{r} - \omega t)\, G(\underset{\sim}{r},t)\, d\underset{\sim}{r}\, dt \quad (1.4b)$$

In the general case the correlation functions G are complex. In the classical domain they are real and have a simple, intuitive significance: given an atom at point $\underset{\sim}{r} = 0$ at time $t = 0$, $G_S(\underset{\sim}{r},t)$ is the probability that <u>the same</u> atom is at distance r at time t, and $G(\underset{\sim}{r},t)$ is the number density of

of atoms [including the atom originally at (0,0)] at position $\underset{\sim}{r}$ at time t. G_S is termed the <u>self correlation function</u> and G the <u>pair correlation function</u>. At time zero

$$G(\underset{\sim}{r},0) = g(\underset{\sim}{r}) + \delta(\underset{\sim}{r})$$
$$G_S(\underset{\sim}{r},0) = \delta(\underset{\sim}{r}) \qquad (1.5)$$

where $g(\underset{\sim}{r})$ is the pair distribution function ordinarily measured with X-rays. For liquids and other isotropic systems only the magnitudes of $\underset{\sim}{r}$ and $\underset{\sim}{Q}$ are significant. The self correlation function for a liquid at sufficiently large times (and therefore distances) is given in terms of the coefficient of self diffusion (D) by the expression (1,3)

$$G_S(\underset{\sim}{r},t) = \pi^{-3/2}(4Dt)^{-3/2}\exp[-r^2/4D|t|] \qquad (1.6a)$$

which has the transform

$$S(Q,\omega) = 2DQ^2/[(DQ^2)^2+\omega^2] \qquad (1.6b)$$

From the behaviour of $G_S(r,t)$ at intermediate times one can deduce the mechanisms by which diffusion occurs (3). At sufficiently small times (and therefore small distances) G behaves <u>in the same way for any system</u> (composed of a particular kind of atom) and is given (1) by the expression which applies for all times for a perfect gas:

$$G_S(r,t) = [2\pi t(k_B T t - i\hbar)/M]^{-3/2}\exp[-Mr^2/2t(k_B T t - i\hbar)] \qquad (1.7a)$$

and correspondingly,

$$S(Q,\omega) = \left(\frac{2\pi M}{k_B T}\right)^{1/2} Q^{-1} \exp\left(-\frac{\hbar\omega}{2k_B T}\right) \exp\left\{-\frac{2\frac{M\omega^2}{Q^2} + \frac{(\hbar Q)^2}{2M}}{4k_B T}\right\} \tag{1.7b}$$

VAN HOVE (1) has shown that the complex functions G can be obtained from the functions S by performing Fourier transformations over the variables Q, ω. Such a transformation has been carried out by BROCKHOUSE and POPE (4) over experimental measurements on liquid lead, a substance which is sufficiently close to being a classical liquid that only the real part of the correlation function is important. For a classical liquid

$$G(r,t) = \frac{1}{2\pi^2}\int_0^\infty i(Q,t)\,\frac{\sin Qr}{Qr}\,Q^2 dQ \tag{1.8a}$$

where $$i(Q,t) = \int_{-\infty}^{\infty} S(Q,\omega)\cos\omega t\, d\omega \tag{1.8b}$$

For a strictly classical liquid (or other isotropic system) $S(Q,\omega)$ is even in ω and only positive (or negative) values of ω need be used in the transformations.

For a general system the functions S for neutron energy gain and loss are connected via the condition for microscopic reversibility (detailed balance) which for most systems in thermodynamic equilibrium is expressed by the condition

$$S(Q,-|\omega|) = S(-Q,-|\omega|)$$
$$= \exp\left(-\frac{\hbar|\omega|}{k_B T}\right) S(Q,|\omega|) \qquad (1.9)$$

SCHOFIELD (5) has proposed redefinitions of G and S which take this fact explicitly into account. EGELSTAFF (6) has emphasized the importance for neutron moderation calculations of insisting that the scattering function satisfy the detailed balance condition. Eq. (1.9) provides a useful check upon the accuracy of experimental results, as do also certain theorems on moments due to PLACZEK (7) and to DE GENNES (8).

To perform the Van Hove transformations information is required over the whole of ω-Q space. However, the asymptotic expressions [Eqs 1.6,1.7] can be used to extrapolate the measurements, if they have been taken into the ranges in which these expressions are valid. A large region of ω-Q space can be covered only when the energies E_o and E' are comparatively large, as is illustrated in Fig. 1 which shows curves of Q vs $\hbar\omega$ for different scattering angles ϕ and two energies E_o. The range of ω-Q space for neutrons of energy 0.005 ev (Be neutrons) is seen to be much more restricted than for neutrons of energy 0.1 ev. For substances with "usual" binding and atomic spacing it is desirable to cover a range of Q from $\sim$0.3 $\mathring{A}^{-1}$ to 10 $\mathring{A}^{-1}$, and a range of energy transfers from $\sim 10^{-4}$ to 10^{-1} ev. Thus to take full advantage of the method it is necessary to use neutrons of rather high energy, though for <u>experimental</u> reasons it may be convenient to do also measurements at low energies.

The primary interest in the classical G(r,t) lies in the fact that it is a sort of "moving picture" of the motions of the atoms in the liquid. At present there does not exist any method of using G(r,t) to compute other quantities of interest, for example the transport properties. Neither does there exist an intuitive interpretation of the imaginary component, nor is it completely clear what is the best way of defining intuitively the classical correlation function when G(r,t) contains a small imaginary component as it does in real liquids. It may be best to think of the ratio of the imaginary/real parts as a measure of the reliability of applying the intuitive interpretation for a classical liquid to the real part of G for an actual liquid. Until these questions are resolved there seems to be little use transforming experimental data except for nearly classical systems.

For most other systems it is necessary to compare the results of calculations based on specific theories with the experimental results, instead of using an inversion procedure. For coherent scattering from single crystals, however, the Born-von Kármán formalism (9) enables the neutron scattering results to be analyzed directly in terms of interatomic forces.* The Born-von Kármán theory will be discussed in the next section.

* A similar formalism for aligned magnetic systems exists in the BLOCH spin wave theory (10), which allows the exchange interactions between the spins of atoms to be deduced from neutron scattering measurements.

2. LATTICE DYNAMICS AND NEUTRON SCATTERING

In the Born-von Kármán theory of lattice dynamics the crystal is considered (9) as a system of mass points which interact with forces obeying Hooke's Law. For a crystal containing N atoms and having one atom per unit cell, there are 3N independent vibrations which are the normal modes of the system. The wave vectors $\mathbf{q}$ of the vibrations range over one zone of the reciprocal lattice. The polarization vectors of the vibrations, $\boldsymbol{\xi}(\mathbf{q})$, are given by a set of three linear equations:

$$4\pi^2 M \nu^2(\mathbf{q})\, \xi_\alpha(\mathbf{q}) = \sum_\beta^3 C_{\alpha\beta}(\mathbf{q})\, \xi_\beta(\mathbf{q}) \tag{2.1}$$

where

$$C_{\alpha\beta}(\mathbf{q}) = \sum_\ell \Phi_{\alpha\beta}(\mathbf{R}_\ell) \exp(i\, \mathbf{q}\cdot\mathbf{R}_\ell) .$$

The ξ_α, ξ_β are components of the polarization vector $\boldsymbol{\xi}$. The indices α,β denote any of three selected, mutually perpendicular coordinate directions. The index ℓ ranges over all the neighbors of a given atom and $\mathbf{R}_\ell$ is the vector distance of the neighbor from the given atom. $\Phi_{\alpha\beta}(\mathbf{R}_\ell)$ is a force constant which gives the force exerted on the given atom in the direction α, when the neighbor at position $\mathbf{R}_\ell$ is moved a unit distance away from its equilibrium position, in the direction β.

Eqs (2.1) have solution for $\underset{\sim}{\xi}$ only when the frequency ν satisfies the equation

$$\left| 4\pi^2 M \nu^2(\underset{\sim}{q})\, \delta_{\alpha\beta} - C_{\alpha\beta}(\underset{\sim}{q}) \right| = 0 \quad . \tag{2.2}$$

Eq. (2.2) is a cubic equation and has three solutions

$$\nu = \nu_j(\underset{\sim}{q}) \tag{2.3}$$

where j = 1 to 3 denotes the branch of the frequency spectrum. To each $(\underset{\sim}{q}, \nu_j)$ there corresponds a polarization vector $\underset{\sim}{\xi}_j(\underset{\sim}{q})$ whose components satisfy Eqs (2.1). In general these components involve the force constants $\Phi_{\alpha\beta}$, and thus are not known a priori. For certain $\underset{\sim}{q}$'s which satisfy symmetry conditions, however, the $\underset{\sim}{\xi}$'s are known.

The frequencies can be determined from neutron spectroscopy measurements, very directly, as is now well known.* In the energy distributions of neutrons scattered coherently by single crystals there are found neutron groups which satisfy the equations for conservation of quasi-momentum and of energy between the neutron and a single phonon, that is,

$$\underset{\sim}{Q} \equiv \underset{\sim}{k}_0 - \underset{\sim}{k}' = 2\pi \underset{\sim}{\tau} - \underset{\sim}{q} \tag{2.4a}$$

$$\hbar\omega \equiv E_0 - E' = h\nu \tag{2.4b}$$

* The possibility of carrying out such experiments appears to have been first realized by J.M. Cassels as early as 1949, but he failed to publish his proposal. The experiments were independently conceived by PLACZEK et al. (11), by the author, and perhaps by others.

where $\underset{\sim}{\tau}$ is a vector of the reciprocal lattice. By means of Eqs (2.4) an observed neutron group can be interpreted to give a pair of values for ν and $\underset{\sim}{q}$ which belong to the frequency-wave number <u>dispersion relation</u> [Eq. (2.3)] of the crystal. Repeated observation of many neutron groups for different incident neutron energies, angles of scattering, specimen orientations, etc. then builds up the dispersion relation, which can be compared with results of calculations for various models of crystal interactions.

This subject has been extensively discussed elsewhere (11-13), and in an accompanying paper (14).

It is attractive, however, to go beyond this and to attempt to use the measured dispersion relation to deduce the interatomic force constants $\Phi_{\alpha\beta}(\underset{\sim}{R}_{\ell})$. It is practically impossible to do this directly by Fourier transformation, not only because of the very large number of values of ν and $\underset{\sim}{q}$ required, but because it is necessary to know the polarization vectors $\underset{\sim}{\xi}_j$ for each mode also. Neither is it possible to determine the Φ's by fitting Eq. (2.2) to the measurements by least squares, since a non-linear least squares fit is required, and one must have a reasonably accurate initial set of values of the Φ's in order to commence the fitting process. It is necessary to start by looking in those positions in reciprocal space for which the directions of the $\underset{\sim}{\xi}_j$ are fixed by symmetry. When $\underset{\sim}{\xi}_j$ is fixed by symmetry Eq. (2.2) factors, and (for a crystal with one atom per unit cell only!) the frequency is

given by an equation which is linear in the force constants. Hence in this case it is possible to carry out a least squares fit.

Consider the situation when $\underset{\sim}{q}$ is in a mirror plane, for convenience taken to be the x-y plane normal to the z direction. Then for one branch, say j = 3, the polarization factor $\underset{\sim}{\xi}_3$ is in the z direction. For the other two branches, $\underset{\sim}{\xi}_1$ and $\underset{\sim}{\xi}_2$ are mutually perpendicular and in the mirror plane, but are not otherwise fixed by symmetry. Eq. (2.2) factors into two equations:

$$4\pi^2 M \nu_3^2 = \sum_{\ell} \Phi_{zz}(\underset{\sim}{R}_\ell) \exp(i \underset{\sim}{q} \cdot \underset{\sim}{R}_\ell) \tag{2.5}$$

and

$$\begin{vmatrix} C_{xx} - 4\pi^2 M \nu_j^2 & C_{xy} \\ C_{xy} & C_{yy} - 4\pi^2 M \nu_j^2 \end{vmatrix} = 0 \tag{2.6}$$

with j = 1, 2.

If $\underset{\sim}{q}$ also lies in a second mirror plane $\underset{\sim}{\xi}_1$ and $\underset{\sim}{\xi}_2$ are also fixed by symmetry. Then Eq. (2.6) again factors and ν_1 and ν_2 also obey equations which are linear in the force constants. Thus measurements in the symmetric directions can be utilized directly to attempt to find the force constants. The number of symmetric directions is very limited however and may not contain sufficient information to enable a complete solution of the problem to be made. This situation has actually

been encountered in the accompanying paper on the Crystal Dynamics of Lead - see ref. (14). It is therefore desirable to obtain the additional information contained in the linear transverse branches in the mirror planes [Eq. (2.5)].

In the usual methods of measurement the crystal is mounted with the mirror plane in the plane of the spectrometers i.e. the plane of the vectors $\underset{\sim}{k}_0$ and $\underset{\sim}{k}$. The transverse branch [Eq. (2.5)] does not contribute to the scattering in this plane because the polarization vector $\underset{\sim}{\xi}_3$ is normal to $\underset{\sim}{Q}$. [The intensity is proportional to $(Q.\underset{\sim}{\xi})^2$.] To study the branch it is necessary to use a different geometry, such as, for example, is shown in Fig. 2. In the figure ORPT represents the plane of the spectrometers. The x-y plane is the mirror plane, with a reciprocal lattice vector $\underset{\sim}{\tau}_M$. T is the reciprocal lattice point. The reciprocal lattice vector $\underset{\sim}{\tau}_M$ is arranged to lie in the plane of the spectrometers, and the crystal is mounted so that it can be rotated about $\underset{\sim}{\tau}_M$. The wave vector of the incoming neutrons ($\underset{\sim}{k}_0$) and the scattering angle (ϕ) are arranged to satisfy the equation

$$|\underset{\sim}{k}_0| \sin\phi = 2\pi |\underset{\sim}{\tau}_M| \quad . \tag{2.7}$$

Under these conditions the vector $\underset{\sim}{q}$ lies in the mirror plane of the reciprocal lattice passing through T, and the polarization vector $\underset{\sim}{\xi}_3$ has a substantial component along $\underset{\sim}{Q}$. Changing the angle χ by rotating the crystal about $\underset{\sim}{\tau}_M$ allows the entire transverse branch in the mirror plane to be studied.

The complete set of values of $(\nu_3, \underset{\sim}{q})$ can be used in least squares fitting along with the results in the symmetric directions, or they can be Fourier transformed to obtain force constants Φ_{zz} between <u>lines</u> of atoms perpendicular to the mirror plane, in the same way as the results for symmetric directions can be transformed to yield interplanar force constants (15, 14).

Finally measurements at general positions in reciprocal space can also be used in the linear least squares fit if a theorem of FOREMAN and LOMER (15) is employed. The theorem states that the three frequencies for a given $\underset{\sim}{q}$ satisfy the relation

$$4\pi^2 M \sum_{j=1}^{3} \nu_j^2(\underset{\sim}{q}) = \sum_{\ell} \left[\Phi_{xx}(\underset{\sim}{R}_\ell) + \Phi_{yy}(\underset{\sim}{R}_\ell) + \Phi_{zz}(\underset{\sim}{R}_\ell) \right] \times \exp(i\, \underset{\sim}{q} \cdot \underset{\sim}{R}_\ell) \qquad (2.8)$$

which is linear in the force constants. A corollary for mirror planes gives

$$4\pi^2 M \left[\nu_1^2(\underset{\sim}{q}) + \nu_2^2(\underset{\sim}{q}) \right] = \sum_{\ell} \left[\Phi_{xx}(\underset{\sim}{R}_\ell) + \Phi_{yy}(\underset{\sim}{R}_\ell) \right] \exp(i\, \underset{\sim}{q} \cdot \underset{\sim}{R}_\ell) \qquad (2.9)$$

To use results at general positions in reciprocal space in a linear least squares fit it is necessary to obtain <u>all</u> the frequencies at the position belonging to branches which are

not fixed by symmetry, and to use the sums of their squares as indicated. This procedure will not give the force constants uniquely, but may usefully supplement the measurements in symmetric directions.

In a crystal with one atom per unit cell it is possible (12) in principle to measure the directions of the polarization vectors $\underset{\sim}{\xi}$ (the eigenvectors), by studying the relative intensities of the neutron groups corresponding to the frequencies at some particular $\underset{\sim}{q}$. This occurs because the intensity of a group is proportional to the quantity $(\underset{\sim}{Q} \cdot \underset{\sim}{\xi})^2$. If the eigenvectors are determined, then the results of measurements at general positions <u>can</u> be used in the linear least squares fits. However, such experiments have not yet been carried out.

For crystals containing n atoms per unit cell the situation is not nearly as satisfactory, as there are usually only a few <u>points</u> in reciprocal space at which the eigenvalues ν^2 are linear in the force constants. One may, however, sometimes use combinations of the squares of frequencies to obtain linear quantities, in order to supplement the linear information available. The difficulty is not completely remedied by study of the intensities, since, in a crystal with more than one atom per unit cell, intensity measurements determine the modulus of a linear combination of the (usually complex) eigenvectors. Thus a problem akin to the phase problem of

crystallography results, and one must determine the polarization vectors for the vibrations at the particular value of $\underset{\sim}{q}$, by computational methods somewhat similar to those used in determining magnetic structures by neutron diffraction. The vectors so determined, together with the frequencies, yield completely linear equations (similar to Eqs. 2.1), even for crystals with many atoms per unit cell. This procedure, which gives promise of being very powerful, will be discussed in detail elsewhere. It will be greatly facilitated by the "constant $\underset{\sim}{Q}$" method of taking measurements, which is discussed in the next section.

Finally the problem of identification of the branch to which an observed phonon belongs must be mentioned. Even for phonons at symmetry points, it is essential that the right equation be attached to a given pair of values of (μ_j, $\underset{\sim}{q}$) when making the fits, so that correct identification is necessary. In many cases the problem is trivial, in others however, recourse must be had to the intensities as a function of the position in the reciprocal lattice (12, 13); i.e. an approximate determination of the eigenvectors must be made.

3. "CONSTANT Q" AND OTHER SPECIAL METHODS*

The natural variables of a scattering experiment are, as we have seen, the wave vector and energy transfers, $\underset{\sim}{Q}$ and ω. If the distribution of the energy of the outgoing neutrons (E') is measured in the ordinary way, at fixed incoming energy (E_0), angle of scattering (ϕ), and specimen orientation (ψ), [Fig. 3], then $\underset{\sim}{Q}$ varies with E' and thus with $\hbar\omega$. Hence $\underset{\sim}{Q}$ cannot be preselected. By changing ϕ and ψ simultaneously as E' (and thus k') is changed it is possible to arrange that $\underset{\sim}{Q}$ remains at a constant preselected value, and thus to measure the distribution of energy transfers at constant $\underset{\sim}{Q}$. This can only be done with crystal spectrometers of course, and not with time of flight apparatus. This fact constitutes an important advantage of the crystal spectrometer method.

The components of $\underset{\sim}{Q}$ in the plane of the spectrometers are given by the equations

$$Q_1 = -k_0 \sin\psi + k' \sin(\phi+\psi)$$
$$Q_2 = k_0 \cos\psi - k' \cos(\phi+\psi) . \qquad (3.1)$$

Given the values Q_1 and Q_2 which are to be held constant, and the fixed value of k_0 (or k') to be used, corresponding values

* This section of the paper was also presented at the Conference on Neutron Diffraction in Relation to Magnetism and Chemical Bonding at Gatlinburg, Tennessee, April 20-22, 1960. See Bull. Amer. Phys. Soc. Ser II. 5, 462 (1960).

of ϕ, ψ, and k' (or k_o) are calculated on a computer. In our own programs (written by Miss M. Millican) we use equal increments of the angle $2\theta_A$ (or $2\theta_M$) which are related to k' (or k_o) respectively through the Bragg law

$$\lambda = 2\pi/k = 2d \sin\theta$$

and compute the corresponding increments in ϕ and ψ necessary to keep $\underset{\sim}{Q}$ constant. These increments, rounded to the nearest $1/8^o$, are applied to the spectrometer.

If the magnitude only of $\underset{\sim}{Q}$ is to be kept constant, as in experiments on liquids, then increments in ϕ only are computed, and ψ is held constant, or is made to vary mechanically as $\phi/2$.

In our present apparatus the increments in ϕ (and ψ) are set up on 52 rotary switches which are connected into the circuit one by one (or two by two) for each point. We can thus take energy distributions of 26 points at constant vector $\underset{\sim}{Q}$, and of 52 points at constant magnitude of $\underset{\sim}{Q}$. An improved apparatus is under construction which will use paper tape as a memory instead of switches. The computed increments in the several variables will be punched onto tape at the computer, and the tape used to control the spectrometers.

It is possible to use approximate linear variations of the parameters to good advantage. If the ratios of the increment in ϕ $[\delta\phi]$ and in ψ $[\delta\psi]$, to the increment in $2\theta_A$ $[\delta(2\theta_A)]$ are computed at some particular point, they may

often also be used in the neighborhood of the point with acceptable accuracy.

For constant k_o, and linear variations in ϕ and ψ as well as in $2\theta_A$,

$$\delta\psi = -\frac{k'}{2k_o}\,\frac{\cot\theta_A}{\sin\phi}\,\delta(2\theta_A)$$

$$\delta\phi = \left[\frac{k_o}{k'}\cos\phi - 1\right]\delta\psi \quad . \tag{3.2}$$

For constant k', and linear variations in ϕ and ψ, as well as in $2\theta_M$,

$$\delta\psi = \frac{\cot\theta_M}{2\tan\phi}\,\delta(2\theta_M)$$

$$\delta\phi = \left[\frac{k_o}{k'\cos\phi} - 1\right]\delta\psi \tag{3.3}$$

In the above formulas the parameters are evaluated at the centre of the distribution to be taken, e.g. at the assumed position of the phonon in the case of a crystal experiment.

Other types of specialized experiments have also been performed:

(a) k' and ϕ (or k_o and ψ) can be simultaneously varied in such a way as to cause the terminus of $\underset{\sim}{Q}$ to move in a specified direction in the horizontal plane. Thus, for example, phonons with $\underset{\sim}{q}$ in a par-

ticular direction can be studied.

(b) If an extremely steep dispersion curve is to be studied it may be advantageous to take distributions in $\underset{\sim}{Q}$ at constant energy transfer. For fixed E_0 and E', ϕ and ψ are varied together in such a way as to cause the terminus of $\underset{\sim}{Q}$ to move in the desired direction in reciprocal space. This method has been used by SINCLAIR et al. (16) to study the dispersion curve of the magnons in a F.C.C. cobalt-8% iron alloy. It was previously used by R. STEDMAN (private communication), who employed mechanical means for obtaining the correlation between ϕ and ψ.

In either case linear variations in the variables can often be used with sufficient accuracy, as in the "constant Q" method.

The various types of experiments are illustrated in Fig. 3 by vector diagrams which represent Eqs (2.4). In all the diagrams the object is to obtain the dispersion curve of longitudinal phonons in the $[\zeta,\zeta,\zeta]$ direction of the reduced zone, and in particular the frequency of the longitudinal phonon at the zone boundary, midway between adjacent reciprocal lattice points.

Diagram OAB shows the conventional experiment in which a neutrons with fixed $\underset{\sim}{k}_0$ (OA) are scattered through a fixed angle (ϕ) into a direction $\underset{\sim}{k}'$. In the conventional experiment $-\underset{\sim}{k}'$ and $\underset{\sim}{q}$ intersect at some arbitrary angle as in diagram OAB. If the neutron group does not appear at B but

instead appears at B', the phonon observed is not in the desired direction. The experiment must then be repeated with new parameters until the neutron group appears at the correct position in reciprocal space. We call this the "Method of Successive Approximations". If $\underset{\sim}{k}'$ falls almost along the direction of $\underset{\sim}{q}$, as in diagram OCD, then a phonon D' obtained in the initial experiment is probably still in the desired direction, and therefore useful.

By changing two variables simultaneously (either k' and ϕ, with k_o and ψ held constant, or k_o and ψ, with k' and ϕ held constant) one can maintain $\underset{\sim}{q}$ in the correct direction, as illustrated by diagrams OEF and OGH.

The constant Q method with k', ϕ, ψ as the independent variables is illustrated by diagram OLM, and with k_o, ϕ, ψ independent by diagram OJK.

In experiments on crystals the constant $\underset{\sim}{Q}$ method has five major advantages:

(a) Data are taken only in regions of reciprocal space in which they are required, thus reducing the amount of experimental work.

(b) In the conventional method $\underset{\sim}{Q}$ changes with E', and thus different neutron groups belonging to different $\underset{\sim}{Q}$'s may merge. Also neutron groups are often sharper with the constant $\underset{\sim}{Q}$ method than with the conventional method, for the same reason.

(c) The intensities of the groups depend only on the frequency, and not (as in the conventional method) also on the gradient of the frequency. [The Jacobian $|J| \equiv 1$ in the expression for the intensities (17, 12, 13). This will be discussed elsewhere in collaboration with A.D.B. Woods.]

(d) The variation with temperature of the phonon frequency for a particular $\underset{\sim}{q}$ is more easily and accurately obtainable with the constant $\underset{\sim}{Q}$ method than with the conventional method. Similarly the widths of the neutron groups for different temperatures are more readily comparable.

(e) When phonons at general points in reciprocal space are to be used in the force constant analysis, it is necessary to make measurements for the 3n frequencies involved [2n if the point is in a mirror plane] at exactly the same position in reciprocal space. [See § 2.] This is obviously much more easily done with the constant $\underset{\sim}{Q}$ than with the conventional method.

In most of our work we now use methods in which the analyzer is kept at a fixed setting and the energy of the incoming beam (E_o) is changed. The intensity of the incoming beam is measured by means of a thin monitor counter, in our case a U^{235} fission counter, whose sensitivity is accurately calculable. The scattered neutrons are counted during the interval in which a fixed, preset number of monitor counts is accumulated, and then E_o is changed to a new value. Since E' is fixed no difficult corrections for the efficiency of the analyzing spectrometer need be applied. Likewise there is no transformation function involved in going from the measured distribution to an energy distribution. The counts are simply plotted as a

function of $\hbar\omega$, giving the energy distribution directly. To the extent that the monitor counter has a "1/v" characteristic, the factor k'/k_0 in Eq. (1.3) is cancelled automatically, and the distribution is directly proportional to the function $S(Q,\omega)$. The small corrections for deviation of the monitor from 1/v behaviour and for contamination in the beam can be easily and accurately applied. Accordingly the constant $\underset{\sim}{Q}$ method with fixed analyzer should give, almost directly, unusually accurate values for $S(\underset{\sim}{Q},\omega)$.

The above method should be especially useful when the Van Hove transformation is to be applied to obtain $G(r,t)$. The necessity for having values for S over the whole of ω-Q space makes for rather severe problems in data handling, particularly in the laborious procedures necessary to obtain $S(Q,\omega)$ from $\sigma(E_0,E',\phi)$. The constant Q method with fixed analyzer entirely eliminates this part of the data handling. The method can be made even more convenient by taking data in constant increments of ω as well as of Q. It is hoped that the method will make the problem of performing the Van Hove transformation much more tractable, as well as make the results more accurate, than with the conventional method.

4. THE TRIPLE-AXIS CRYSTAL SPECTROMETER

If the unique power inherent in neutron inelastic scattering studies is to be fully realized it is essential that the apparatus used cover a wide range of the energies, E_0 and E', and of the angular parameters, ϕ and ψ. It is also desirable that the resolution be readily changeable, since in some experiments the pattern may be intense but require examination at high resolution, and in other experiments the pattern may be weak in which case comparatively poor resolution must be used.

The triple-axis spectrometer was designed to be as flexible and generally useful as possible. The schematic diagram is shown in Fig. 4, which illustrates the general layout and the nomenclature used. Photographs of the spectrometer in various aspects are shown in Figs. 5 to 7.

The spectrometer is located at the NRU reactor which has a central flux of $\sim 3 \times 10^{14}$ n cm^{-2} sec^{-1}, at an experimental hole of elliptical cross section [about 8 cm wide by 10 cm high] which penetrates to the reactor core. The flux seen by the spectrometer is believed to be almost 2×10^{14} n cm^{-2} sec^{-1} at the source. The spectrometer is located at a distance of about 6 meters from the source, and therefore the maximum angular apertures available are $\sim 1^{\circ}$.

The spectrometer has the following valuable features:

(a) The incoming energy E_0 is continuously and reproducibly variable over wide ranges. The angle $2\theta_M$ is continuously variable over 35° ranges, with a maximum angle of 92° and a minimum angle of 0°.

(b) The reflecting planes of the monochromating and analyzing crystals can be quickly and reproducibly changed.

(c) The collimators C_2, C_3, and C_4 [Fig. 4] can be readily changed, without disturbing the alignment of the crystals. [Note that this includes the collimator (C_2) on the reactor side of the monochromator.]

(d) The ranges of the variables are large: from 0° to 92° for $2\theta_M$, from 0° to 100° for $2\theta_A$, and from 0° to about 130° for ϕ.

(e) The spectrometer can be converted almost instantly to a conventional double-axis diffraction instrument.

The beam size normally used is 5 cm x 5 cm, though provision has been made for increasing this to 6.5 cm x 6.5 cm. The angular apertures are fixed by inserting Soller-slit collimators at the various positions indicated in Fig. 4. In practice collimators are usually inserted at one of C_2 and C_3, and at one of C_4 and C_5.

The spectrometer has been gradually assembled in the course of five years, largely on the basis of actual experience.

The four principal components will be described in turn:

A. The monochromator facility which produces the monoenergetic neutron beam.

B. The positional spectrometer which sets the angles ϕ and ψ.

C. The analyzing spectrometer which measures the outgoing energy.

D. The control units and recording apparatus.

Following this, brief discussions will be given of:

E. The monochromating crystals.

F. The use of the instrument.

A. The monochromator facility

The monochromator facility comprises the shielding, collimators and mechanism for the monochromating crystal (X_1), a large moveable platform which carries the positional and angular spectrometers, and an accurate scale by which the angle $2\theta_M$ can be read. The facility is designed primarily to be used as a crystal spectrometer, but can also be used as the basis for a double chopper time-of-flight spectrometer, or for a rotating crystal spectrometer. The detailed design of the facility was carried out by McALPIN (18). It was completed in January 1960, but had been used in an incomplete state since the inception of experimental work at NRU in November 1958.

The range of the drum angle $2\theta_M$ is from 32° on one side of zero to 92° on the other, in continuous ranges of -32° to $+2^\circ$, -2° to $+32^\circ$, 28° to 62°, and 58° to 92°. This is

accomplished by using two concentric drums, the inner of which has two holes (through which collimator C_3 can pass) the two holes being separated by 60°. The outer drum has four similar holes separated by 30°. The collimator C_3 passes through one selected pair of holes, the others being plugged. By coupling the holes together in different combinations, the different angular ranges are covered. An open wedge at the reactor side of the drum allows the drum to move with respect to the collimator C_2 and permits continuous variation within the range. The open wedge is well shielded by the yoke at all orientations.

The drum is mechanically coupled to a moving platform whose angular position can be read on an accurate scale of large radius [see Figs. 5-7]. The platform (and drum) can be electrically driven in $1/8^o$ steps, thus changing $2\theta_M$.

The monochromating crystal (X_1) follows the turning of the drum at half its angular speed, thus keeping the crystal aligned and the Bragg relation satisfied. The half-angling mechanism will be discussed later in connection with the analyzing spectrometer. The crystal is connected to the half-angling mechanism by a magnetic clutch, and is also connected by a second magnetic clutch to a control unit outside the shielding. The control unit can be used to align the crystal with the angle $2\theta_M$ held fixed at some convenient position. The magnetic clutch connecting the crystal to the control unit is then de-energized and the crystal connected to the half-angling mechanism by the other magnetic clutch. The control unit is equipped with an

accurately machined index plate see Fig. 8a which allows different planes of the monochromating crystal to be brought into the Bragg position, without the necessity for realignment.

The collimator C_2 is mounted on a separate moveable carrier, which can be rotated around through an angle of 90° from its usual position in order to change the collimator. The drum wedge, of course, also rotates.

The drum and the yoke each have large holes, H_1 and H_2, 30 cm in diameter. at their centres. In normal operation an auxiliary gate is located in H_1, which is closed when it is desired to work in the diffracted beam. The extra space around the crystal in H_2 is usually filled with extra shielding. However a chopper or cooled filter could be located in H_1, and a second chopper or rotating crystal unit could be placed in H_2, thus converting the unit to a time-of-flight spectrometer. H_2 could also be used to hold a magnet for polarized neutron experiments.

Monitor counters are located in the incoming (M_1) and outgoing (M_2) neutron beams, to record the white neutron, and monoenergetic neutron intensities see Fig. 4. . Counter M_1 is a natural uranium fission counter and M_2 is an enriched U^{235} fission counter (19).

Fig. 8b shows a trace of the counting rate in monitor counter M_2 as the angle $2\theta_M$ is changed linearly in time. The trace gives the reactor spectrum as modified by crystal reflectivity and parisitic reflections.

B. <u>The positional spectrometer</u>

The positional spectrometer is basically the unit described by HURST et al. (20). It consists of a heavy arm

whose angular position (ϕ) is indicated directly on an accurate scale, and an accurately indexed table (ψ) which can be coupled to the arm through a half-angling mechanism [a belt and pulley system]. The spectrometer arm can be driven electrically in $1/8^{\circ}$ steps, by a motor, cam and belt system. The indexed table can be arranged to half-angle, or it can be independently driven in $1/8^{\circ}$ steps.

C. <u>The analyzing spectrometer</u>

The analyzing spectrometer is mounted directly on the arm of the positional spectrometer. The analyzing crystal is mounted on an indexed table permanently connected to the arm of the analyzing spectrometer through a half-angling mechanism. The arm is driven electrically in $1/8^{\circ}$ steps, at an angular speed of eleven degrees/minute, by means of two worm-gear assemblies. There is no mechanism for decoupling the spectrometer from the worm drive and all movements are made electrically. The motor, mounted at the end of the spectrometer arm, is connected to the worm-gear drive through a magnetic clutch. The magnetic clutch is activated for the brief time necessary to go through the $1/8^{\circ}$ cycles.

The half-angling mechanism consists of three bearings (whose axes make angles of 120°), which are rolled between a plate which moves with the arm ($2\theta_A$) and a plate which is fixed in space. The crystal table is carried on shafts which pass through the centres of the bearings. Since the diameter of the bearing is twice its radius, the crystal table moves at half the angular speed of the arm, as required.

The design of this unconventional but successful spectrometer was carried out by C.A. CRAWFORD. It has been in use since 1956.*

The counters used are enriched BF_3 (96%B^{10}) counters, which are irradiated through one end. The counters are 6.2 cm in diameter, with an active length of 25 cm, and a dead length at the window of 3.7 cm. Counters with BF_3 pressures of 5 cm, 15 cm, 30 cm, 45 cm and 60 cm are available. Care is taken to select a counter suitable for the wavelength range to be studied, and particularly to be sure that the counter used does not contain any more boron than is necessary. [Excess boron contributes to the fast neutron background but not appreciably to the signal .] The counters were constructed by the Chalk River Counter Development Section headed by I.L. FOWLER.

D. <u>The control units and recording apparatus</u>

The control units provide the following sequence of operations:

1. The spectrometers are set up manually with the four parameters $2\theta_M$, $2\theta_A$, ϕ, and ψ at their initial positions. One at least of the parameters is fixed. The numbers of $1/8^\circ$ increments by which the other (moving) parameters

---

* Prior to this time, spectrometer B was used as the analyzing spectrometer and the angle of scattering was set by the relative positions in space of the specimen and the analyzing spectrometer [see refs (3),(12)].

will advance, are selected.

2. The spectrometers advance to their first positions.

3. Counting takes place at the first position. The number of counts accumulated in the signal counter for a preset number of monitor counts (in M_2), is recorded. The counting period may be repeated without change if desired, or repeated with insertion of a cadmium shutter between M_2 and S [Fig. 4] to measure background, or repeated with the analyzing crystal turned out of the Bragg position for a different kind of background measurement. If the net signal is much smaller than the background, signal and background counts are recorded for equal periods. If the signal is considerably the larger, two signals and one background period of equal duration may be used. If the signal is very large, background is often omitted. For magnetic experiments counting may be carried out with a magnetic field applied to the specimen, and with the magnetic field removed.

4. After completion of the operations at the first positions of the parameters, the spectrometers advance by the preselected increments again, counting is repeated, and so on through a preset number of positions.

At the conclusion of the set of measurements (for some types of experiments), the spectrometers can be made to move to new initial positions, and a new set of measurements carried out automatically. Where the increments by which the

parameters advance are the same for each position (linear operation), the number of positions is virtually unlimited. For non-linear operation the number of positions is at present limited to 26 or 52, as discussed in § 3, and one set only can be carried out automatically. The new paper-tape control unit under construction will enable any number of positions to be used, and any number of non-linear experiments to be performed automatically in sequence.

Most of the detailed design of the control units was carried out by C.E.L. GINGELL and by E.A. GLASER.

The recording apparatus is mostly conventional. Streeter-Amet traffic counters were used until recently. A number of pens were added to indicate directions of travel, signal or background, magnet on, etc. Recording is now done on an electric typewriter and tape punch, using a unit designed by W.D. HOWELL, who also designed the new paper tape control unit.

A simple histogram plotter is used for visual purposes. The plotter consists of a modified commercial counting rate meter and a recording potentiometer. The resistor is removed from across the accumulating capacitor in the counting rate meter, thus converting it to an integrator. The capacitor and its immediate circuitry are replaced by low leakage components. Teflon-insulated contacts, operated by a relay, can be made to short the capacitor. During the counting period the motor on the recording potentiometer is shut off, and the potentiometer pen draws a horizontal line whose length is pro-

portional to the number of accumulated counts. At the conclusion of the counting period the motor is turned on briefly, and then the capacitor is shorted out by the relay contacts restoring the pen to zero. The motor continues to run for another brief period, thus completing the histogram plot.

A set of plots of the energy distributions of neutrons scattered by liquid lead (4), as recorded on the histogram plotter, is shown in Fig. 9. Most of the distributions were taken in sequence by the spectrometer without attention, the angle ϕ being increased by 6° between each distribution taken up to $\phi = 96^{\circ}$. Starting with $\phi = 99^{\circ}$, the process was then reversed.

E. The monochromating crystals

The monochromating crystals used are cut from single crystal ingots of aluminum 6.2 cm diameter x 30 cm long, which are grown in graphite crucibles by the Bridgeman method. Occasionally lead crystals cut from similar ingots are also used. The aluminum crystals typically have rocking curves of from 0.5° to 0.7° full width at half maximum, which admirably match the widths of our collimators.

The monochromating crystal (X_1) normally used, is cut as an approximate cylinder of 5.5 cm diameter by 6 cm high, the axis of the cylinder being in the $[1\bar{1}0]$ direction of the crystal. The cylindrical axis is set vertical. The crystal can then be oriented in the horizontal plane so that

the (111), (002), (220), (113), (331) planes can be brought into Bragg reflection position by means of the control unit discussed in B [Fig. 8a].

A similar crystal mounted on an index plate similar in principle to the one shown in Fig. 8a, is often used as the analyzing crystal. [See Figs 5-7.] We also use aluminum and lead crystals cut in the Fankuchen manner to reflect from (111) planes. These crystals are mounted on pre-aligned plates which are keyed in such a way that they may be secured to the analyzing spectrometer without alignment being necessary (see Fig. 7).

We use aluminum crystals for strictly practical reasons. Of the crystals that have been available to us up to now, they have had the highest reflectivity for our conditions. (a) The best balance of intensity and resolution is usually secured with collimators of aperture between $1/2^{\circ}$ and 1°. It is desirable on one hand that the mosaic width of the crystal be no greater than the collimation, or neutrons reflected by the crystal will be intercepted by the collimators, and on the other that the crystal have the maximum possible reflectivity, thus indicating a large mosaic width. The mosaic widths for our aluminum crystals match the requirements for our collimators. (b) The long mean free path in aluminum enables cylindrical crystals of 5.5 cm diameter to be used, which would be more difficult with, say, lead or copper.

F. Use of the instrument

In using the instrument we normally work at the lowest practical energies in order that the resolution may be as high as possible with a given set of crystals and collimators However there are difficulties involved in using low energies, because of the effects of higher order reflections by the crystals. These effects can sometimes be eliminated or reduced by the use of filters.

Polycrystalline beryllium filters are ideal where they can be used, but there are not many experiments in which both E_0 and E' can be kept below the beryllium cut-off (5×10^{-3} ev). However, if E_0 is below the cut-off and E' is sufficiently large that the second order energy (4E') falls outside the energy distribution of the scattered neutrons, then a single beryllium filter in the incoming beam suffices. Similarly if E' is below the cut-off and E_0 is near or above the peak of the reactor spectrum then a single beryllium filter can be employed. In many cases, however, the higher of the two energies falls in the region in which overlap of the spectra (seen in the first and second orders of the crystal) occurs. The new single crystal quartz filters (19, § 6) are highly useful in this range, and we have employed them at first order energies as low as 0.012 ev. Actually, a considerable amount of order contamination can often be tolerated, particularly with phonon experiments where measurements are required only on particular neutron groups which can often be kept away from

parts of the distribution which involve order effects. (However, the order contamination still upsets the intensity calibrations, and the intensities must be corrected.)

The filters are usually inserted at position C2 of Fig. 4, using the collimator carrier described in § 4A which allows them to be inserted or removed without affecting the crystal alignment, and at position C5. In these positions the filters assist in reducing the background as well as the order contamination.

Normally we use good collimation at C3 and C4 in order to define the directions of $\underset{\sim}{k}_o$ and $\underset{\sim}{k}'$ accurately, with poorer collimation at C2 and C5. With this arrangement the directions of $\underset{\sim}{k}_o$ and $\underset{\sim}{k}'$ do not depend much upon the alignment of the monochromating crystals X_1 and X_2. (From the point of view of background reduction, however, it would be preferable to use the better collimation at C2 and C5, and we actually used this arrangement for several years.) We usually operate with open collimators tapering to 6.2 cm square in C1 and C2, and with appropriate Soller slit collimators (cadmium) at C3 and C4. A coarse Soller slit collimator is used at C5, into which beryllium slabs can be fitted when a beryllium filter is required. With this collimator in place, background can be measured by turning the analyzing crystal (X_2) a few degrees out of the Bragg position.

In order to conserve intensity we usually employ Soller slits for which the vertical divergences are limited only by the

beam size. The vertical divergence is then set by the overall dimensions of the beam and the specimen, and the physical separation of the components, and amounts to roughly 3° for both the incident and outgoing beams. This represents a compromise between the requirements for specimens (such as liquids) which scatter isotropically about the incoming beam, and for crystals which scatter anisotropically. For liquids the vertical divergence does not affect the resolution or accuracy, except possibly at small angles of scattering. For crystals the vertical divergence is now usually the most important contributor to the error, since it results in a small shift in the energy of the neutron group arising from the second derivative of the frequency/wavevector relation normal to the plane of the spectrometers. Since we usually make measurements in the mirror planes of the crystal, for which the first derivative is zero, the vertical divergence does not much affect the resolution.

We normally try to arrange that the resolution for the incoming and outgoing neutrons be approximately the same, by using a coarser collimator and a plane of larger spacing with the lower energy of the two (E_0 and E') than with the higher.

Every effort is made to keep the background low, since it is often the controlling influence on the experiments. The counter is selected according to the energy range, for best signal/background ratio. Boron carbide and cadmium shielding surrounds the analyzing crystal X_2, and, except for the crystal,

the counter "sees" only this shielding. A considerable amount of auxiliary shielding is often used which is simply piled about the various parts of the apparatus. In normal operation the background ranges from one to four counts per minute.

We now use almost exclusively the procedure in which the outgoing energy E' is fixed for a given set of experiments, and the incoming energy E_0 is varied. The incoming beam is monitored by the thin fission counter M2, whose response is almost 1/v, and counting is conducted for a preset number of monitor counts. This procedure eliminates the analyzer sensitivity from consideration, and makes the intensities more accurate and (as we saw in §3) almost directly proportional to $S(\underset{\sim}{Q}, \omega)$. Because the counting rate in the incoming beam varies widely, (see Fig. 8b), the counting time also undergoes wide changes, and therefore so do the counts recorded from the background. It is therefore almost essential in this procedure that the background be recorded point-by-point with the signal, and this is nearly always done.

5. The Rotating Crystal Time-of-Flight Spectrometer

The rotating crystal spectrometer (22) is a member of the class of pulsed-beam spectrometers in which a pulsed monoenergetic beam of neutrons is scattered by a specimen, and the energy distributions of the neutrons scattered through various angles are measured by time-of-flight. In general, pulsed-beam spectrometers are capable of higher resolution for a given intensity than are crystal spectrometers. (However they do not permit the constant $\underset{\sim}{Q}$ method nor the other special methods to be used.) The rotating crystal instrument is the simplest and cheapest of the pulsed-beam spectrometers, but it has a number of peculiarities which operate both to its advantage and disadvantage. In the sections following we will discuss the following topics:

A. General principles of operation of the rotating crystal spectrometer.

B. The present Chalk River rotating crystal spectrometer.

C. Theory of the instrument.

D. Use of the instrument.

A. General Principles of operation

In the three years since the first rotating crystal spectrometer was set up at the NRX reactor, several versions have been used for various experiments at Chalk River. A schematic diagram of the apparatus now in use at the NRU

reactor is shown in Fig. 10. A single crystal rotates about a vertical shaft, at a comparatively high angular velocity, in our case at 8000 r.p.m. Each time a crystal plane comes into position for Bragg reflection a burst of monoenergetic neutrons, with energy given by the Bragg law, is sent down the collimator and impinges on the specimen. The scattered neutrons are observed by means of several counters at different angles of scattering, and their energies after scattering are determined from their times-of-flight over the known distances from the specimen to the counters.

The method has several attractive features:

(a) The equipment is comparatively simple and cheap, and is rugged and reliable.

(b) Backgrounds are low since the monoenergetic beam is deflected away from the line of the experimental hole.

(c) There is no time-dependent fast neutron background.

(d) The pulsed monoenergetic beam can have a larger area than is readily obtainable with beams produced by mechanical means.

(e) As in other pulsed-beam time-of-flight methods, measurements may be made simultaneously at several angles of scattering, thus enhancing the counting rate.

(f) Burst-focussing properties sometimes enable long on-time to be used without spoiling the resolution.

As in crystal spectrometers order contamination exists in the monoenergetic beam. If the rotating crystal produces only two bursts per revolution (i.e. if a single plane is used) then it can be arranged that the only contaminant pulses will be those from the higher orders of the plane used. If, however, four or six bursts per revolution are produced, then other planes necessarily also come into reflecting position, and contaminate the beam. For example, we have used an aluminum crystal with its [111] axis vertical, which produces six bursts per revolution from {220} planes, but which also produces six bursts from {422} as well as from {440} planes. There are thus contaminant bursts of 3 times the nominal energy, as well as the usual order contamination of 4 times the first order energy.

In addition to order contamination, the beam contains neutrons diffusely scattered by the rotating crystal and its shield. These neutrons have a distribution of energies, and are scattered continuously in time, so they produce a flat background which is almost time-independent. This white contamination is much more important with a rotating crystal than with an ordinary crystal spectrometer, because the Bragg-scattered neutrons are reflected only for a small fraction of the time (say 1%) while the diffusely-scattered neutrons are produced all the time. It is therefore very important that a crystal for use in a rotating crystal spectrometer should have little incoherent scattering. It should

also have a melting temperature >> room temperature, so that thermal diffuse scattering can be kept small. (A high melting point is also desirable from the point of view of mechanical strength.)

All order contamination could be removed, and the white contamination reduced, by passing either the incident or diffracted beam through a coarse chopper phased with the rotating crystal so as to pass first order neutrons. At some cost in intensity, but with an improvement in resolution, this could also be accomplished by reflecting the beam again from another rotating crystal phased with the first. Filters may also be used, as in normal crystal spectrometers. At present the instrument is being used with neutrons of wavelength longer than the beryllium cut-off, and a liquid-nitrogen-cooled beryllium filter eliminates the order contamination.

In common with all pulsed-beam spectrometers the instrument suffers from frame overlap. It is not clear, a priori, with what initial neutron burst a detected neutron is to be identified. Hence the time-of-flight of a neutron is ambiguous to the extent that any integral number of repetition times may be added to the nominal time-of-flight. Frame overlap for a given spectrum can be almost eliminated by reducing the repetition rate of the monoenergetic pulses, but usually only at a considerable cost in intensity. It can be corrected for in several ways which will be discussed later.

Especially at long wavelengths, the operation of the instrument is influenced by the Doppler shifts in the neutron velocities produced by the crystal rotation. These are correlated with the positions in the crystal at which reflection took place, since different parts of the crystal have different velocities. The shifts can sometimes be used to compensate for the uncertainty in the time of origin of the burst, which is introduced by the dimensions of the rotating crystal. Furthermore as the crystal rotates the length of the path followed by the neutron may change in time, as may also the reflected wavelength. Thus there is the possibility of burst-focussing, (22) since neutrons reflected at different times with different wavelengths in different parts of the crystal can be made to arrive at the counter simultaneously.

Because planes of high multiplicity can be used (of up to six in a cubic crystal) the repetition rate of the pulses can be high with quite moderate speeds of rotation.

The rotating crystal spectrometer is inherently a high resolution instrument since, if the instrument is to be efficient, the collimation must approximately match the effective mosaic width of the crystal. This width is usually not large, nor can a crystal of very large mosaic width be profitably used even if one were available, because of the resulting low peak reflectivity. Thus the angular apertures are kept small, the burst time short, and the resolution high.

B. The present Chalk River instrument

At present the instrument is set up at one of the elliptical holes which penetrate the NRU reactor core, similar to the hole used by the triple-axis crystal spectrometer (§4). The rotating crystal is mounted on a lathe bed set parallel to the line of the neutron beam (see Fig. 10). A mechanical linkage between the centre of the mount for the rotating crystal and the specimen table keeps the collimator correctly oriented. Thus, except for necessary changes in the shielding, the wavelength is continuously variable. A filter, cooled to liquid nitrogen temperature, is located within the reactor shielding. For wavelengths $>4\mathring{A}$ a filter consisting of 40 cm of polycrystalline beryllium plus 30 cm of quartz single crystals (21) is used. (The quartz is cheaper than the beryllium, and supplements it for fast neutron and γ-ray shielding.) For wavelengths $<4\mathring{A}$ filters consisting of several quartz crystals with a total length of up to 80 cm are used. In addition a single crystal of lead 6.5 cm in thickness is sometimes included to assist in the suppression of γ-rays. The filters will be discussed in more detail in §6. With these filters in the path of the beam, only nominal shielding is required around the rotating crystal and to stop the beam.

The rotating crystals used up to now have been aluminum spheres about 6 cm in diameter which were cut from single crystal ingots on a lathe. They were then oriented in the desired way, and a 0.63 cm hole drilled through the

sphere along the axis of rotation. The crystal was then mounted on a threaded shaft and held by means of lock-nuts. The assembly was then trimmed in a lathe to balance it. The crystal and its shaft are mounted in a cylindrical shield, with the shaft passing through self-aligning bearings in the ends of the shield. The shaft is flexibly coupled to a commercial* hysteresis synchronous motor, which operates from a

---

* Manufactured by The Electric Indicator Co. Inc., Stanford, Connecticut, U.S.A.

---

115 volt 400 cycle supply. A six pole motor gives a speed of 8000 r.p.m. and a four pole motor 12000 r.p.m. The motor drives a mirror with the appropriate number of faces to produce pulses in a photomultiplier each time a crystal plane comes into reflecting position. The pulses from the photomultiplier start the timing circuits of the electronics to measure the times-of flight of the neutrons.

The reflected bursts of neutrons pass through a collimator (C2), a thin monitor counter (M2), and then impinge on the specimen. The neutrons scattered by the specimen are observed in a set of three detectors, which are located within a massive shield mounted on a trolley at a distance of 3.3 metres from the specimen. The trolley moves on a set of tracks, the wheels of the trolley having the correct conical camber to maintain the alignment of the counters. Detailed design of the unit was carried out by W. BEALE. A photo-

graph of this part of the apparatus is shown in Fig. 11.

Two sets of enriched $B^{10}F_3$ detectors are used: (a) In one set each of the detectors is made up of two cylindrical counters 6.5 cm in diameter and 50 cm long, arranged vertically. Thus each detector has a width of $\sim$12 cm, corresponding to a horizontal divergence of $\sim 2^{\circ}$, and a height of 50 cm, corresponding to a vertical divergence of $\sim 9^{\circ}$. The average thickness along the flight direction is $\sim$5 cm. These detectors are used to study liquids and other materials for which, since they scatter isotropically about the direction of the incoming neutrons, the vertical divergence has little effect. (b) The other set of detectors is used for studies in which the resolution in $\underset{\sim}{Q}$-space is important. In this set each detector is a cylindrical counter 6 cm in diameter and 12 cm high, so that the horizontal divergence is $\sim 1^{\circ}$ and the vertical divergence $\sim 2^{\circ}$. The detectors are separated by angles of about 2.5°. The flight path for the central detector is made slightly shorter than for the other two, in order to assist in the determination of the frame to which neutron groups belong. The use of three closely spaced detectors allows phonon frequencies in specified directions in $\underset{\sim}{q}$-space to be determined accurately by interpolation without excessive use of the method of successive approximation.

The counters in set (a) contain BF_3 gas (enriched to 96% B^{10}) at 60 cm pressure, and those in set (b) contain

similar gas at 73 cm pressure. (For time-of-flight work it is desirable to have small dimensions in the direction of flight, and therefore the highest pressures which are compatible with good pulse characteristics are desirable. At the time these counters were constructed these pressures were as high as were readily obtainable.) The efficiencies of the counters range from about 0.15 at 1Å to about 0.4 at 4Å. They were calculated under various assumptions as to the extent of the "dead space" close to the wall of the counter. The absolute magnitude of the sensitivity changed considerably according to the assumed dead space, but the relative wavelength variation of the sensitivity varied by only a few percent. Thus the sensitivity curves of our counters are probably known to a few percent over the entire wavelength range from 0 to 7Å, but normalization procedures must be carried out to obtain absolute values for cross sections.

The shielding of the counters consists of about 2.5 cm of pressed boron carbide immediately surrounding the detector volume in the massive shield (Fig. 11), with about 30 cm of a mixture of $(CH_2)_n$ and borax outside the boron carbide. The shielding is designed on the principle that as little moderating material as possible should be within, or included in, the inner boron carbide shield. A massive collimator, constructed on similar principles, conducts the neutrons from the specimen to the detectors. Except for the specimen, the shielding is arranged so that the detectors see

only a surface of cadmium behind which is boron carbide. The general background is about 2 counts per minute in a single detector of set (a), and is much less in a detector of set (b).

The monitor counters (M1 and M2) are fission counters using single foils of natural uranium.

The time elapsed between the light pulse from the rotating crystal and the detection of the neutron, together with the identification number of the counter in which the neutron was detected, are recorded as a four digit number in coded decimal form on punched tape. Thus the number 3127 means that a neutron was detected in counter #3 at a time 127 channel widths after the light pulse. Channel widths of from 2 to 20 μsecs are available. The individual events are then sorted into a set of time distributions on a computer. While the numbers are in the computer simple arithmetical operations can be performed, such as corrections for background or for sensitivity. The time-to-punch converter was designed by ROBINSON et al and is described in detail elsewhere (23). The programs for the Datatron computer were written by J.M. KENNEDY.

The counting rate is limited by the mechanical read-out and punch system, which has a "dead time" of 0.8 seconds. Thus the instrument is suitable only for experiments in which the counting rate is considerably less than one count/second. This, however, fits in fairly well with the philosophy of the rotating crystal spectrometer, which is inherently a

high resolution/low intensity device.

In addition to the several detector channels, the output of the monitor counter M2 (Fig. 10), and of a shielded background detector, are often also recorded on the punched tape. The time-sorted monitor output allows accurate normalization of the measured distributions to be carried out (even in the presence of noise in the monitor channel), thus automatically correcting for pile fluctuations and for the instrument dead time.

C. Theory of the Instrument

In this section the qualitative aspects of the theory of the instrument will be considered. The complete theory involves integrations over the geometries of the collimators, specimen and rotating crystal, and over the mosaic width of the crystal. To begin, we make the following observations:

(a) As in all time-of-flight spectrometers, the thickness of the counters introduces an uncertainty in the flight path, and thus worsens the resolution of the instrument.

(b) As in all pulsed-beam spectrometers, the resolution also depends on the shape, size and orientation of the specimen, except at a scattering angle $\phi = 0$.

(c) Similarly, the resolution of the rotating crystal spectrometer involves the shape and size of the rotating crystal, and also its mosaic spread and velocity of rotation.

Let us consider first a perfect point crystallite located at the centre of the rotating crystal (point A in Fig. 12(a)), and assume that the collimation before and after the crystal are the same. Then, at the peak of the burst all points in the source (O'OO") contribute to the burst; ray O'A is Bragg reflected by plane BAE as AV", OA as AV, and O"A as AV'. For clockwise rotation (with the beam reflected to the right as in Fig. 12(a)), the burst begins with ray O'A being reflected from plane B'AE' as AV', and ends with ray O"A being reflected as AV". Thus, with equal collimation before and after the rotating crystal, the <u>mean</u> angle of scattering does not change as the crystal goes through the reflecting position since angle O'AV' = OAV = O"AV", and therefore (to first order) neither does the <u>mean</u> wavelength.

The burst time is

$$\delta_1 t_1 = \delta_c / \omega_M \qquad (5.1)$$

where ω_M is the angular velocity of the crystal, and δ_c is the aperture of one of the two equal collimators.

The spread in times-of-arrival of neutrons with the mean energy at the counter (P) depends on the relative path lengths for the rays, and thus on the shape and orientation of the specimen, on the angle of scattering, and on the change in velocity on scattering. If the path lengths of the various rays have an equal length, then the spread is given by Eq. (5.1). If we arrange that path AV"P is

shorter than AV'P (as in Fig. 12(a)), then the neutrons reflected early in the burst must travel further than those reflected late in the burst. Thus neutrons reflected at different times in the burst can be made to arrive simultaneously at the counter, and burst focussing occurs. With a plane specimen arranged in the symmetric position in transmission (Fig. 12(a)) the differences in path lengths are given by the expression

$$\delta L_1 = \delta L_2 \approx L_1 \delta_c \tan \phi/2$$

where L_1 is the flight path between the rotating crystal and the specimen, and L_2 between the specimen and the counter. The difference in times of arrival is

$$\begin{aligned} \delta_2 t_1 &= \delta L_1 / v_0 + \delta L_2 / v' \\ &= L_1 \delta_c \tan \phi/2 \left(1/v_0 + 1/v' \right) \quad . \end{aligned} \tag{5.2}$$

The spread in times of arrival of neutrons of the mean energy is thus

$$\delta t_1 = \left| \delta_1 t_1 - \delta_2 t_1 \right| \quad . \tag{5.3}$$

If the direction of rotation were reversed, the minus sign in Eq. (5.3) would be changed to plus, and defocussing rather than

focussing of the burst would occur.

It will be noted that the degree of burst focussing depends on the angle of scattering, and is zero in the forward direction.

The spread in times of arrival due to the velocity spread of the reflected neutrons must be folded with t_1, that is added approximately root-mean-square. From the Bragg Law the spread in velocity of the neutrons <u>reflected at the peak of the burst</u> is

$$\delta v_A = v_0 \, \delta_c \cot \theta_M \quad .$$

The total spread in the time of arrival is therefore approximately given by

$$\delta t_2 \simeq 0.7 \left\{ L_1 \frac{\delta v_A}{v_0^2} + L_2 \frac{\delta v'}{(v')^2} \right\}$$

$$= 0.7 \, \frac{\delta_c \cot \theta_M}{v_0} \left\{ L_1 + L_2 \left(\frac{v_0}{v'} \right)^3 \right\}$$

where the factor 0.7 takes approximate account of the fact that there is little velocity spread in the neutrons reflected at the beginning and end of the burst. In the derivation the facts that $E' = E_0 + \hbar\omega$, and therefore that $\delta E' = \delta E_0$, are used.

There is a spread in time-of-arrival due to the finite thickness of the detector (Δ_D) which is given by the expression

$$\delta t_3 = \Delta_D / v' \quad . \tag{5.5}$$

Up to now we have considered a perfect crystal. If the crystal has a mosaic spread (δ_M) then there is a spread in time-of-arrival

$$\delta t_4 = \delta_M / \omega_M \quad . \tag{5.6}$$

Since the spreads δt_1, δt_2, δt_3, δt_4 are independent, the overall spread is obtained approximately by adding them root mean square.

If one of the collimators is larger than the other, then the mean velocity is no longer completely independent of the time of origin. Thus for a beam reflected to the right and clockwise rotation, as in Fig. 12(a), with the outgoing collimator (V'AV") larger than the incoming collimator (O'AO"), the neutrons reflected early in the burst have lower mean velocities than those reflected late in the burst, and focussing occurs. Conversely, if the incoming collimator is the larger defocussing occurs. Reversing the directions of rotation reverses the effects.

The finite size of the crystal introduces several important and correlated effects:

(a) Neutrons reflected from the left hand side of the crystal, say at B, must traverse a greater distance than those reflected, say, at E, and this tends to introduce a time spread.

(b) The mean angle of reflection OBT is greater than OEX and therefore neutrons reflected at B tend to be slower than neutrons reflected at E.

(c) Neutrons reflected at points away from the centre of the crystal undergo a change in velocity because of Doppler shift due to the motion of the crystal. Furthermore, with Doppler shift the angle of incidence in the laboratory system does not

equal the angle of reflection, and thus a shift in the time of origin of the burst also occurs. For example, with clockwise rotation neutrons reflected at B come off with <u>increased</u> velocity due to the Doppler shift, but at a <u>later time</u> than would be the case if the motion could be neglected. Thus the two aspects of Doppler effect tend to cancel one another. The velocity shift is usually the larger effect, and thus can also be made to cancel effects (a) and (b) to a large extent.

We will now consider the Doppler effects in more detail. We define a vector $\mathbf{K}$ related to the crystallite velocity $\mathbf{v}_M$ by the equation

$$\mathbf{K} = \frac{m_N}{\hbar}\mathbf{v}_M = \frac{m_N}{\hbar}\boldsymbol{\omega}_M \times \mathbf{R}_M \tag{5.7}$$

where $\boldsymbol{\omega}_M$ has positive sign for clockwise rotation, and $\mathbf{R}_M$ is the position of the crystallite in the rotating crystal. The components of $\mathbf{K}$ in the plane which are parallel and perpendicular to $\mathbf{Q}$ are denoted by $\mathbf{K}_Q$ and $\mathbf{K}_N$ respectively, where $\mathbf{K}_Q$ is positive when it has the same sense as $\mathbf{Q}$. In the development which follows, $\mathbf{k}_{oL}$ and $\mathbf{k}'_L$ are respectively the incoming and outgoing wave vectors in the laboratory system, $\mathbf{k}_{om}$ and $\mathbf{k}'_m$ are the same quantities in the moving system, and $\mathbf{k}_{oS}$ and $\mathbf{k}'_S$ are the same quantities with the crystal stopped. We can write immediately

$$\mathbf{k}_{om} = \mathbf{k}_{oL} - \mathbf{K}$$

$$\mathbf{k}'_m = \mathbf{k}'_L - \mathbf{K}$$

and, for Bragg scattering,

$$\underset{\sim}{k}_{oM} - \underset{\sim}{k}'_M = \underset{\sim}{k}_{oL} - \underset{\sim}{k}'_L = \underset{\sim}{k}_{oS} - \underset{\sim}{k}'_S = 2\pi \underset{\sim}{\tau}.$$

The appropriate reciprocal space diagram is shown in Fig. 13. Since the angle of scattering ($2\theta_M$) is fixed, the terminus of $\underset{\sim}{k}_{oL}$ must always be on the arc of the circle which passes through the origin (O), the terminus of $\underset{\sim}{k}_{oS}$ (U) and the reciprocal lattice point (P), from the well known theorem in geometry.

We observe first, that the only effect of the component $\underset{\sim}{K}_N$ is to change the vectors k_{oM} and k'_M, and thus the wavelength and the angle of scattering in the moving system. This introduces a change in the integrated reflectivity of the crystal, but has no other effect, and we will henceforth restrict attention to the component $\underset{\sim}{K}_Q$.

<u>For small crystal velocities</u>, the outgoing wave vector with the crystal moving is easily seen to have the magnitude

$$\left|\underset{\sim}{k}'_L\right| = \left|\underset{\sim}{k}'_S\right| \mp \left|\underset{\sim}{K}_Q\right| \sin\theta_M , \qquad (5.8)$$

where the sign is positive when $\underset{\sim}{K}_Q$ has the opposite sense to $\underset{\sim}{Q}$ and negative when it has the same sense.

[The vector k_{oL} is given by the similar expression

$$\left|\underset{\sim}{k}_{oL}\right| = \left|\underset{\sim}{k}_{oS}\right| \pm \left|\underset{\sim}{K}_Q\right| \sin\theta_M ,$$

but this fact is of little importance since it indicates only the particular original wavelength selected out of the white incident spectrum. The intensity is, of course, dependent on

the number of neutrons of wave vector $\underset{\sim}{k}_{oL}$ in the original spectrum, so the effect might become of importance if the spectrum varied rapidly, for example at wavelengths near a filter cut-off.]

The vectors $\underset{\sim}{k}_{oL}$ and $\underset{\sim}{k}'_L$ of Fig. 13 satisfy the Bragg condition for the angle $2\theta_M$, but the vectors are not parallel to $\underset{\sim}{k}_{oS}$ and $\underset{\sim}{k}'_S$, (i.e. to the collimators). Thus the reciprocal space diagram (the crystal) must be rotated around O until $\underset{\sim}{k}_{oL}$ becomes coincident with $\underset{\sim}{k}_{oS}$ and $\underset{\sim}{k}'_L$ parallel to $\underset{\sim}{k}'_S$, as indicated by construction OR'P' in Fig. 13. The rotated vectors $\underset{\sim}{k}_{oL}$ and $\underset{\sim}{k}'_L$ are denoted respectively by $\underset{\sim}{k}_{oT}$ and $\underset{\sim}{k}'_T$. Physically, this means that the orientation of the crystal for Bragg scattering is different when it is moving from when it is still. For small crystal velocity, the change in angle is given by the expression

$$\delta \psi_M = |\underset{\sim}{K}_Q| \cos \theta_M \,/\, |\underset{\sim}{k}_{oS}| \tag{5.9}$$

and is clockwise when $\underset{\sim}{K}_Q$ is negative, i.e. antiparallel to $\underset{\sim}{Q}$, as in Fig. 13.

To return to the problem of the Doppler shifts in the apparatus of Fig. 12(a), we identify the new vector $\underset{\sim}{k}'_T$ with $\underset{\sim}{k}_o$, the wave vector of the neutrons selected by the rotating crystal and incident on the specimen. Fig. 13 is an exaggerated representation of the situation at point B in Fig. 12(a), except that there $\underset{\sim}{K}_N = 0$. To avoid integrations we consider separately the problem along the orthogonal directions perpendicular and parallel to $\underset{\sim}{Q}$ (BAE

and GAC respectively in Fig. 12(a)), and then combine the time spreads for the two directions by root mean square addition.

We consider first positions along the line GAC, for which $\underset{\sim}{K_Q}$, and therefore the Doppler effect, is zero. The burst occurs at the same time for all points along this line. The mean angle of reflection (OGW) for point G is different, however, from the mean angle (OAV) for point A, by an amount

$$\delta_G\ (2\theta_M) = R_M\ \cos\theta_M / L_o$$

where R_M is the distance GA, an appropriate mean radius of the rotating crystal, and L_o is the distance between the rotating crystal and the source. The difference in the mean velocities of neutrons reflected from G and A is therefore, from the Bragg Law,

$$\delta v_G \equiv v_G - v_A = - v_o R_M \cos^2\theta_M / L_o \sin\theta_M \ . \tag{5.11}$$

The path differences for neutrons scattered at G and A are:

$$\begin{aligned} \delta L_{1G} &\equiv GW - AV = + R_M\left(\sin\theta_M - \cos\theta_M \tan(\phi/2)\right) \\ \delta L_{2G} &\equiv WP - VP = - R_M \cos\theta_M \tan(\phi/2) \ . \end{aligned} \tag{5.12}$$

The equations for point C are the same as (5.11) and (5.12) except that the signs of the right hand sides are reversed.

The time spread in the arrival at the counter between neutrons reflected at C and at G is therefore

$$\delta t_5 = 2\left| \frac{-\delta v_G}{v_0^2}\left\{L_1 + L_2\left(\frac{v_0}{v'}\right)^3\right\} + \frac{\delta L_{1G}}{v_0} + \frac{\delta L_{2G}}{v'} \right| \tag{5.13}$$

We now consider points in the crystal along the line BAE, for which K lies along Q. For clockwise rotation the velocities of neutrons scattered at point B are increased by Doppler effect over those of neutrons scattered at A, by an amount

$$\delta v_D = \omega_M R_M \sin\theta_M \tag{5.14}$$

from Eqs. (5.7) and (5.8). The burst at B occurs later than at A by a time

$$\delta t_D = \delta\psi_M / \omega_M = R_M \cos\theta_M / v_0 \tag{5.15}$$

from Eqs. (5.7) and (5.9). It is to be noted that this shift in the burst origin is independent of the angular velocity.

The mean angle of scattering at B is greater than at A by an amount

$$\delta_B(2\theta_M) = R_M \sin\theta_M / L_0 \tag{5.16}$$

resulting in a difference in velocity of

$$\delta v_B = - v_0 R_M \cos\theta_M / L_0 \quad . \tag{5.17}$$

The path differences are given by the expressions

$$\begin{aligned} \delta L_{1B} &\equiv BT - AV = R_M \left(\cos\theta_M + \sin\theta_M \tan(\phi/2) \right) \\ \delta L_{2B} &\equiv TP - VP = R_M \sin\theta_M \tan(\phi/2) \quad . \end{aligned} \tag{5.18}$$

The equations for point E are the same as (5.14) to (5.18) except that the signs on the right hand side are reversed.

The time spread between the arrival at the counter of neutrons reflected from B and from E is given by the equation

$$\delta t_6 = 2 \left| - \frac{\delta v_B + \delta v_D}{v_0^2} \left\{ L_1 + L_2 \left(\frac{v_0}{v'} \right)^3 \right\} + \delta t_D + \frac{\delta L_{1B}}{v_0} + \frac{\delta L_{2B}}{v'} \right| \quad . \tag{5.19}$$

The time distributions are usually divided into channels of finite width (δt_7) which contributes to the resolution.

Where the specimen material has an especially small cross section, appreciable thicknesses of specimen material must be employed, and this worsens the resolution by an amount

$$\delta t_8 \simeq \Delta_s \sec(\phi/2) \left| 1/v_0 - \cos(\phi)/v' \right| \tag{5.20}$$

where Δ_S is an appropriate mean thickness for the specimen.

In studying effects of the finite crystal size we assumed that the outgoing vector $\underset{\sim}{k}'_T$ was in a fixed direction, that is, that Soller slits of small aperture were used in the outgoing beam. The Soller slits actually have an aperture δ_c and this introduces a time spread. Consider points in the vicinity of A in Fig. 12(a). Some of these will see the Soller slits from a position near the edge of a slit, whereas we have implicitly assumed that A was at the centre of a slit. This gives rise to additional spreads in the burst time (of magnitude $\delta c / 2\omega_M$) and in the velocities (of δv_A), which are correlated with each other and with a variation in path length similar to that already discussed for point A. The spread in burst time (for clockwise rotation) is found by methods similar to those already used, to be given by the expression:

$$\delta t_q = \left| \frac{-v_0 \delta_c \cot\theta_M}{v_0^2} \left\{ L_1 + L_2 \left(\frac{v_0}{v'}\right)^3 \right\} + \frac{\delta_c}{2\omega_M} - L_1 \delta_c \tan\phi/2 \left(1/v_0 + 1/v' \right) \right| \qquad (5.21)$$

The factor 2 in the denominator of the second term arises because the ray reflected from the rotating crystal moves at twice the angular speed of the crystal.

The total resolution width is approximately given by the R.M.S. sum of the individual widths

$$\delta t = \left[\sum_{i=1}^{9} (\delta t_i)^2 \right]^{1/2} \tag{5.22}$$

where δ_c, δ_M, R_M, and Δ_D are chosen in a compatible way, for example as full widths at half maximum.

In the preceding development we assumed that all parts of the crystal are equally effective in reflecting neutrons, that is, we neglected extinction. In fact extinction will usually be important, particularly at long wavelengths. It is interesting to note that <u>extinction is not as important in a rotating crystal as in the same crystal when still</u>, because in traversing the crystal the neutron encounters material in different states of motion and thus at different points along the path of the neutron the conditions in the laboratory system for Bragg reflection are different. Thus the increased resolution width caused by Doppler effect is accompanied by increased intensity. In fact, in some conditions it may be possible to use quite perfect crystals in a rotating crystal spectrometer, and still obtain good efficiency.

If a thin, flat crystal were employed instead of a sphere, it would be possible to select the angular velocity and geometry in such a way as to compensate completely the effects of the finite size of the rotating crystal. The crystal

could also be cut so that the faces were oriented with reference to the reflecting plane in such a way as to achieve focussing in space, as with Fankuchen-cut crystals in ordinary crystal spectrometers. Thus narrow beams of high resolution and high intensity are obtainable. Using a flat crystal, however, eliminates the benefits to the intensity from Doppler effect, and using space-focussing eliminates the burst-focussing feature found with flat specimens.

The resolution is dependent on the scattering angle, and the shape and orientation of the specimen. Therefore if the resolution is important, it is necessary to measure it for each experimental situation using elastic scattering from an incoherent scatterer of size, shape, and orientation similar to those of the specimen.

We conclude this section by presenting some illustrative computations on the spectrometer of Fig. 10, which was described in § 5B. This arrangement was designed to operate at wavelengths of 1.5Å to 4Å, but most of the work to date has been done at the long wavelength limit at 4.05Å. In table I the various component time widths are presented for this spectrometer for wavelengths 4Å ($v_0 = 10^5$ cm/sec) and 2Å ($v_0 = 2 \times 10^5$ cm/sec), using the following parameters: $L_0 = 690$ (cm), $L_1 = 87$, $L_2 = 330$, $R_M = 1.5$, $\Delta_D = 3$, $\omega_M = 836$ (rad/sec), $\delta_c = 0.007$ (rad), $\delta_M = 0.01$, $2\theta_M = 120^\circ$. The parameters R_M, δ_c and Δ_D were chosen as half the maximum

value in each case, and δ_M is the full width at half maximum of the rocking curve of the crystal used. Computations are presented for elastic scattering ($v' = v_0$), and for large energy gain ($v' \to \infty$). It will be observed that all the contributions are appreciable under at least one of the conditions, and that the magnitudes of most of the components change considerably with the experimental conditions.

As we have already seen, reversing the direction of rotation changes the sign of components of $\delta t_1, \delta t_6, \delta t_9$. The importance of using the correct direction of rotation is illustrated by Fig. 12(b), which shows the elastic incoherent scattering by vanadium, with the crystal rotating clockwise, and anticlockwise. A slightly lower speed of rotation would have given better results on the whole, since this would have decreased the Doppler effect term (δt_6) and δt_9 more than it would have increased δt_1 and δt_4.

Measured resolution widths using 20 μsec channels are in good agreement with the calculations. The measured widths at half maximum for a thin vanadium specimen and 4.05Å neutrons, decrease from 76 μsec at $\phi = 15^\circ$ to 60 μsec at $\phi = 90^\circ$, compared with calculated values of 65 and 44 μsecs respectively. The measured width of the distribution with the counter in the specimen position is 60 μsecs. This should be compared with the value of 48 μsecs calculated for $v' \to \infty$ with an additional width of the form of Eq. (5.5) due to the counter thickness. All these are with the crystal rotating clockwise. With the crystal rotating anti-clockwise ($\phi = 60^\circ$) the measured width at half maximum of the distribution was 174 μsecs, compared with a calculated value

of 139 μsecs. By using larger but still reasonable values for the parameters $[\Delta_D = 4$ cm, $R_M = 1.8$ cm, $\delta_c = 0.01$ radian and $\delta t_7 = 14$ μsecs$]$ almost exact agreement with experiment for the various widths can be obtained.

The preceding theory is, of course, only approximate, especially since most of the resolution elements do not have the Gaussian shape required for combination by R.M.S. addition.

Finally it should be mentioned that D.A. O'CONNOR (24) has also treated the theory of the instrument, without, however, taking into account either Doppler effect or the correlations between resolution elements, and that G.C.E. LOW (private communication) has independently pointed out the correlation between the resolution elements in δt_1.

D. Use of the Instrument

We will illustrate the use of the instrument by means of a distribution measured by SAKAMOTO et al. (25) for 4.05Å neutrons scattered through an angle of 75° by a thin flat specimen of water at 25°C. This is one a series of about 40 patterns taken at 25°C and at 75°C, which are to be used to obtain the self-correlation function of the protons by means of a VAN HOVE transformation. The distribution (Fig. 14) extends over 177 channels, each of approximately 20 μsec width, and one frame is shown in the right hand side of the figure.

If a counter is placed at the specimen position the pattern shown at inset (a) is obtained centred near channel

92. This actually belongs in the preceding frame, and gives the origin of the time-of-flight scale. The pattern is shown relocated at (b) in the preceding frame. The section of the water pattern between channels 92 and 177 may in principle belong in either frame, or may be a mixture of components from each frame, so it is plotted (c) in both frames. [In principle, of course, any part of the pattern may also belong to a still later frame, but in this case this is not a realistic possibility.]

With a 2.5 mm thick, flat specimen of vanadium, pattern (d) is obtained. This is elastic scattering, so the centre of the line gives the mean wavelength of the incoming radiation, and the shape of the line gives the resolution function.

The horizontal line just above the abscissa gives the time independent background when the incoming beam is cut off with cadmium.

To separate the frames for a continuous spectrum such as this, two procedures have been used. (a) With a polycrystalline beryllium filter placed between the specimen and the detector, pattern (e) is obtained. Since only neutrons with $\lambda' > 3.96$Å can pass the filter, the filtered pattern contains only neutrons in the second or succeeding frames. Thus the broad maximum in channels 130-150 belongs in the first frame, and is in fact the "hindered rotation" peak (3) at $\sim$ 0.06 ev energy gain. An approximate separation of frames is shown by the smoothed dashed curve. An exact separation can be made by doing quantitative

work with the filters. (b) The separation can also be made when the complete set of experiments to obtain $S(Q,\omega)$ have been carried out, by using Eqs. (1.9) which relates the intensities for energy gain and energy loss at the same Q and which will only be satisfied if the frame separation has been made correctly.

Sharp peaks in the energy distribution can be assigned to the correct frame easily by repeating the measurements with either a flight path of different length, or with a different speed of rotation of the crystal, and thus with a different frame repetition rate.

Corrections must be applied for the order contamination and the white contamination in the beam. In this case the order contamination was negligible and the white contamination amounted to about 3% of the beam. The contamination is determined from the spectrum seen by the counter placed at the specimen position. Since the white contamination is nearly time-independent it is readily subtracted.

Finally, we interpolate here a few remarks upon the significance of the patterns, which were given in the discussions on water, Session III of the Conference. The author earlier (3) presented measurements showing that a quasi-elastic component exists in the energy distribution of the neutrons scattered from water. This component however was found to be not truly elastic, but to have an energy width. A theory of the width (W) was presented which related it to diffusion in

the liquid, and it was pointed out that the behaviour of the width as a function of Q gave rather detailed information about the modes of diffusion in the liquid. In particular, if diffusion proceeds only by "small" motions (jitter) as opposed to "jumps" of atomic dimensions, then $W = \hbar DQ^2$. It was found that although W increased with Q at roughly the required rate, its absolute magnitude was smaller than calculated, and the conclusion was drawn that although "small" motions contributed to the diffusion some "jumps" must also occur.

Recently however HUGHES et al. (26) presented measurements using the filtered-beam, chopper method, from which they claimed that no diffusion broadening existed but that there were small satellite lines at an energy transfer of 5×10^{-4} ev. The positions at which these lines should appear are shown in Fig. 14 by the arrows A. The resolution used by HUGHES et al. was the same as that used previously by the author, 3×10^{-4} ev. The resolution in the new experiments of SAKAMOTO et al. is 2×10^{-4} ev. No trace of the satellite lines proposed by HUGHES et al. was observed in any of the patterns. In every case diffusive broadening of the "elastic" component was observed, which behaved qualitatively exactly as previously described (3).

6. SINGLE CRYSTAL FILTERS

The total cross section of a single crystal for slow neutrons can be much less than the sum of the cross sections of its constituent atoms. On the other hand the cross section for neutrons with energies in the electron volt to Kev range is just the sum of the individual cross sections. Hence single crystals can operate as useful filters to pass preferentially low energy neutrons (21), while stopping faster neutrons, and perhaps also γ-rays. Since the cross section in the thermal neutron energy region is strongly energy dependent, single crystal filters can also be used to eliminate order effects in crystal spectrometers. The requirements are:

(a) The constituent atoms should have very small capture and incoherent scattering cross sections, and should not be paramagnetic.

(b) There should be no structural disorder in the crystal which could give rise to diffuse scattering.

(c) Large and perfect single crystals should be available. The requirement that the crystals be perfect (have little mosaic spread) ensures that the dips in transmission for neutrons with the proper energy to undergo Laue reflection should not be too pronounced [see, for example, Fig. 8].

(d) The Debye temperature and melting temperature should be high in order that thermal diffuse scattering may be kept small without the necessity of cooling the crystal to liquid helium temperatures.

(e) The cross sections of the constituent atoms for fast neutrons (in the Mev range) should not be anomalously low compared with the cross sections for slow neutrons.

(f) Preferably the atoms composing the crystal should be of high atomic number in order that the cross section for γ-rays should be high.

The essential condition (a) is satisfied primarily by beryllium, bismuth, quartz, and less well by lead. Large single crystals are obtainable only for the last three. Quartz satisfies well all the requirements except (f - discrimination against γ-rays) which it meets only moderately well. Bismuth and lead are very similar, and both are excellent for γ-rays, but bismuth is preferable because it has a smaller capture cross section for neutrons than has lead. In addition, lead single crystals tend to be rather imperfect. (The author does not have any information on the degree of perfection obtainable with bismuth.) Both bismuth and lead have rather low melting points, and hence do not satisfy condition (d) very well. Thus, for most purposes, the author believes that quartz is probably superior to bismuth except when discrimination against γ-rays is particularly important. This statement applies with the crystals at temperatures down to liquid nitrogen temperatures; if liquid helium temperatures could be used bismuth crystals would be decidedly preferred to quartz (21) (except possibly for requirement (c)). As it is, we generally use quartz crystals.

Our quartz crystals are large (10-20 cm) natural crystals which, because of small defects, have been rejected for use as

crystal controls or transducers. They are cheap and still satisfactory for the purpose.

We have measured the cross section of a quartz single crystal in two (unknown) orientations over the energy range 0.037 ev to 0.16 ev using a crystal spectrometer, with the quartz at room temperature ($296^{o}K$) and at liquid nitrogen temperature ($87^{o}K$). The lengths of the crystals in the beam in the two orientations were 6.3 cm and 12.6 cm respectively. The two orientations gave substantially the same results, which are plotted as the heavy lines in Fig. 15(a). The measurements were not extended to lower energies because of order contamination in the beam, and because at the lower energies the specimens were too thin to give accurate results at the low temperature. However, using the capture cross section and other information as a guide we have extrapolated the low temperature curve to cover a wider energy range.

The measurements for room temperature are in good agreement with results of RUSTAD et al. (27) which are shown in Fig. 15(a) as the dashed line, and which cover a wider energy range and are probably more accurate than our results.

In Fig. 15(b) similar curves computed from the cross sections of the component atoms for high energy neutrons (28) and for γ-rays (29) are shown as functions of the energy. The spectra of fast neutrons and γ-rays from reactors both comprise principally energies below ~ 4 Mev. It is seen that quite good discrimination can be obtained for neutrons $\gtrsim 0.05$ ev.

We use quartz crystals at room temperature (of from 5 to 25 cm length) for second order elimination, when operating at energies between 0.013 ev and 0.03 ev. For example at 0.02 ev, 20 cm of quartz reduces the 2nd order neutrons by a factor of $\sim$ 11 and the first order by a factor of $\sim$ 2.5, thus affording discrimination against 2nd order by a factor of $\sim$ 4.5.

We have used filters of up to 70 cm in length at liquid nitrogen temperature with very satisfactory results. With 70 cm of quartz the cadmium ratio was so high that it could not be accurately measured, but values of $\sim 10^5$ were recorded.

Crystals have been used for several months at the outer edge of the reactor shielding (flux $\sim 3 \times 10^9$ n/cm^2 sec) without apparent loss of effectiveness, though severe blackening of the crystals occurred. The crystals did not become appreciably radioactive.

7. ACKNOWLEDGMENTS

Many people have made contributions to the work outlined in this paper, especially D.G. Hurst, who introduced me to the subject of neutron physics, and my collaborators over the years, T. Arase, G. Caglioti, W. Cochran, D.G. Henshaw, P.K. Iyengar, N.K. Pope, M. Sakamoto, R.N. Sinclair, A.T. Stewart, and, not least, A.D.B. Woods. G.M. James and other members of the reactor operations group have been unfailingly cooperative. J.M. Kennedy has given unstinted help in solving computing problems, and E.A. Glaser and others provided indispensable technical assistance.

The idea of the rotating crystal spectrometer arose in a discussion with Dr Hurst. I am grateful to Dr Pope and Dr Woods for a careful reading of the paper.

REFERENCES

1. VAN HOVE, L. Phys. Rev. 95, 249-62 (1954).
2. BROCKHOUSE, B.N. Proceedings of the Neutron Thermalization Conference, April 28-30, 1958, Gatlinburg Tennessee, ORNL-2739 paper IIa. (Abstract only)
3. BROCKHOUSE, B.N. Suppl. Nuovo Cimento Ser X, 9, 45-71 (1958). Phys. Rev. Letters 2, 287-9, (1959).
4. BROCKHOUSE, B.N. and POPE, N.K. Phys. Rev. Letters 3, 259-62 (1959).
5. SCHOFIELD, P. Phys. Rev. Letters 4, 239-40 (1960).
6. EGELSTAFF, P.A., unpublished report.
7. PLACZEK, G. Phys. Rev. 86, 377-88 (1952).
8. DE GENNES, P.G. Physica 25, 825-839 (1959).
9. BORN, M. and HUANG, K., Dynamical Theory of Crystal Lattices, Oxford University Press, London (1954). Chapter V.
10. BLOCH, F. Z.Physik 61, 206-19 (1930).
11. PLACZEK, G. and VAN HOVE, L. Phys. Rev. 93, 1207 (1954).
12. BROCKHOUSE, B.N. and STEWART, A.T. Phys. Rev. 100, 756-7 (1955); Revs. Modern Phys. 30, 236-49 (1958).
13. BROCKHOUSE, B.N. and IYENGAR, P.K. Phys. Rev. 111, 747-54 (1958).
14. BROCKHOUSE, B.N., ARASE, T., CAGLIOTI, G., SAKAMOTO, M., SINCLAIR, R.N., and WOODS, A.D.B. Paper I/S 21
15. FOREMAN, A.J.E. and LOMER, W.M. Proc. Phys. Soc. (London) B 70, 1143-50 (1957).
16. SINCLAIR, R.N. and BROCKHOUSE, B.N., Phys. Rev. 120, 1638 (1960).

17. WALLER, I. and FROMAN, P.O., Ark Fys 4, 183-9 (1952).

18. M^cALPIN, W. The Monochromating Facility for the Chalk River Triple-Axis Neutron Spectrometer, Atomic Energy of Canada Limited report CRGP 956 (1961).

19. M^cKENZIE, J.M., Nucleonics 17, 60-5 (1959).

20. HURST, D.G., PRESSESKY, A.J., and TUNNICLIFFE, P.R., Rev. Sci. Instr. 21, 705-12 (1950).

21. BROCKHOUSE, B.N., Rev. Sci. Instr. 30, 136-7 (1959).

22. BROCKHOUSE, B.N., Bull. Amer. Phys. Soc. Ser II, 3, 233, SP2 (1958).

23. ROBINSON, L.B. and HOWELL, W.D., Transistorized Counting Systems 9. Punched Tape Timesorter, Atomic Energy of Canada Limited report CREL 775 (1960). Issued as AECL No. 989.

24. O'CONNOR, D.A., Nucl. Instr. 8, 244-8 (1960).

25. SAKAMOTO, M., BROCKHOUSE, B.N., JOHNSON, R.H., POPE, N.K., unpublished.

26. HUGHES, D.J., PALEVSKY, H., KLEY, W., and TUNKELO, E. Phys. Rev. Letters 3, 91-3 (1959); Phys. Rev. 119, 872-81 (1960).

27. RUSTAD, MELKONIAN, HAVENS, TAYLOR, GOULD, and MOORE, to be published. See also RAINWATER, L.J., HAVENS, W.W., Jr., DUNNING, J.R. and WU, C.S., Phys. Rev. 73, 733-41 (1948).

28. HUGHES, D.J. and SCHWARTZ, R.J., Neutron Cross Sections, 2nd Ed. BNL 325, (1958).

29. Handbook of Chemistry and Physics, 39th Ed., Chemical Rubber Publishing Co. (1958) p. 2460.

Table I

Calculated time spreads in microseconds for the spectrometer of Fig. 10 with parameters given in the text. Components 1, 2 and 9 are directly proportional to δ_c, components 5 and 6 to R_M, and component 3 to Δ_D. The mean spread (δt_7) due to the channel width of the 20 μsec channels was taken to be 10 μsecs.

	$v_o = 10^5$ cm/sec, $\lambda_o = 4$Å		$v_o = 2 \times 10^5$ cm/sec, $\lambda_o = 2$Å	
	$v' = v_o$	$v' = \infty$	$v' = v_o$	$v' = \infty$
δt_1	$\lvert 8.4 - 12 \tan(\phi/2) \rvert$	$\lvert 8.4 - 6 \tan(\phi/2) \rvert$	$\lvert 8.4 - 6 \tan(\phi/2) \rvert$	$\lvert 8.4 - 3 \tan(\phi/2) \rvert$
δt_2	11.8	2.5	5.9	1.2
δt_3	30	0	15	0
δt_4	12	12	12	12
δt_5	$\lvert 31 - 30 \tan(\phi/2) \rvert$	$\lvert 27 - 15 \tan(\phi/2) \rvert$	$\lvert 16 - 15 \tan(\phi/2) \rvert$	$\lvert 13 - 7.5 \tan(\phi/2) \rvert$
δt_6	$\lvert -51 + 52 \tan(\phi/2) \rvert$	$\lvert 13 + 26 \tan(\phi/2) \rvert$	$\lvert -3 + 26 \tan(\phi/2) \rvert$	$\lvert 11 + 13 \tan(\phi/2) \rvert$
δt_9	$\lvert -12.7 - 12.2 \tan(\phi/2) \rvert$	$\lvert +0.7 - 6 \tan(\phi/2) \rvert$	$\lvert -4.2 - 6 \tan(\phi/2) \rvert$	$\lvert 2.5 - 3 \tan(\phi/2) \rvert$

A.E.C.L. Ref. # A-2599-B

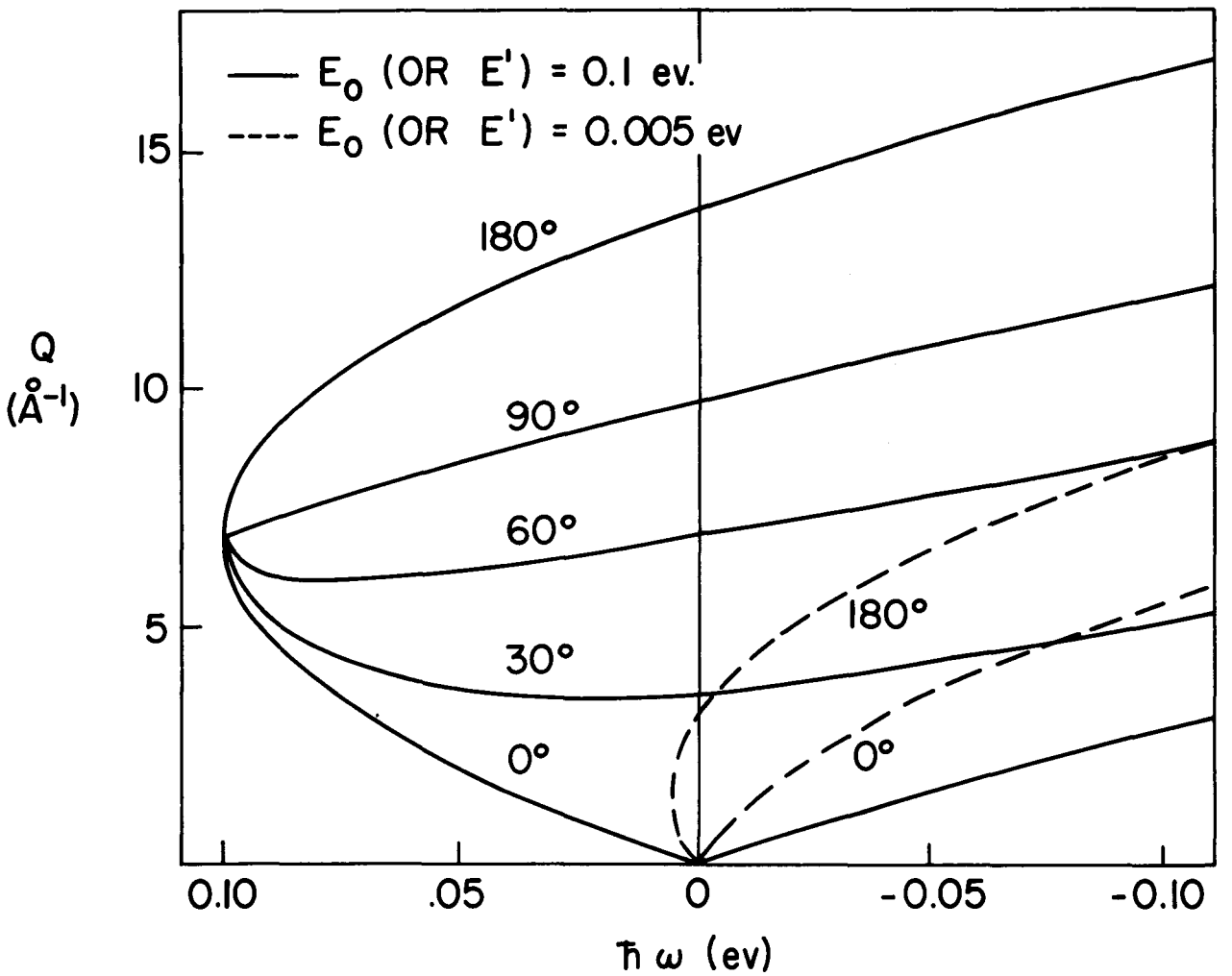

Fig. 1 The wave vector transfer Q as a function of the energy transfer $\hbar\omega$ for two incident energies (E_0) and several angles of scattering. The curves are the same using outgoing energies E', except that the sign of $\hbar\omega$ is reversed.

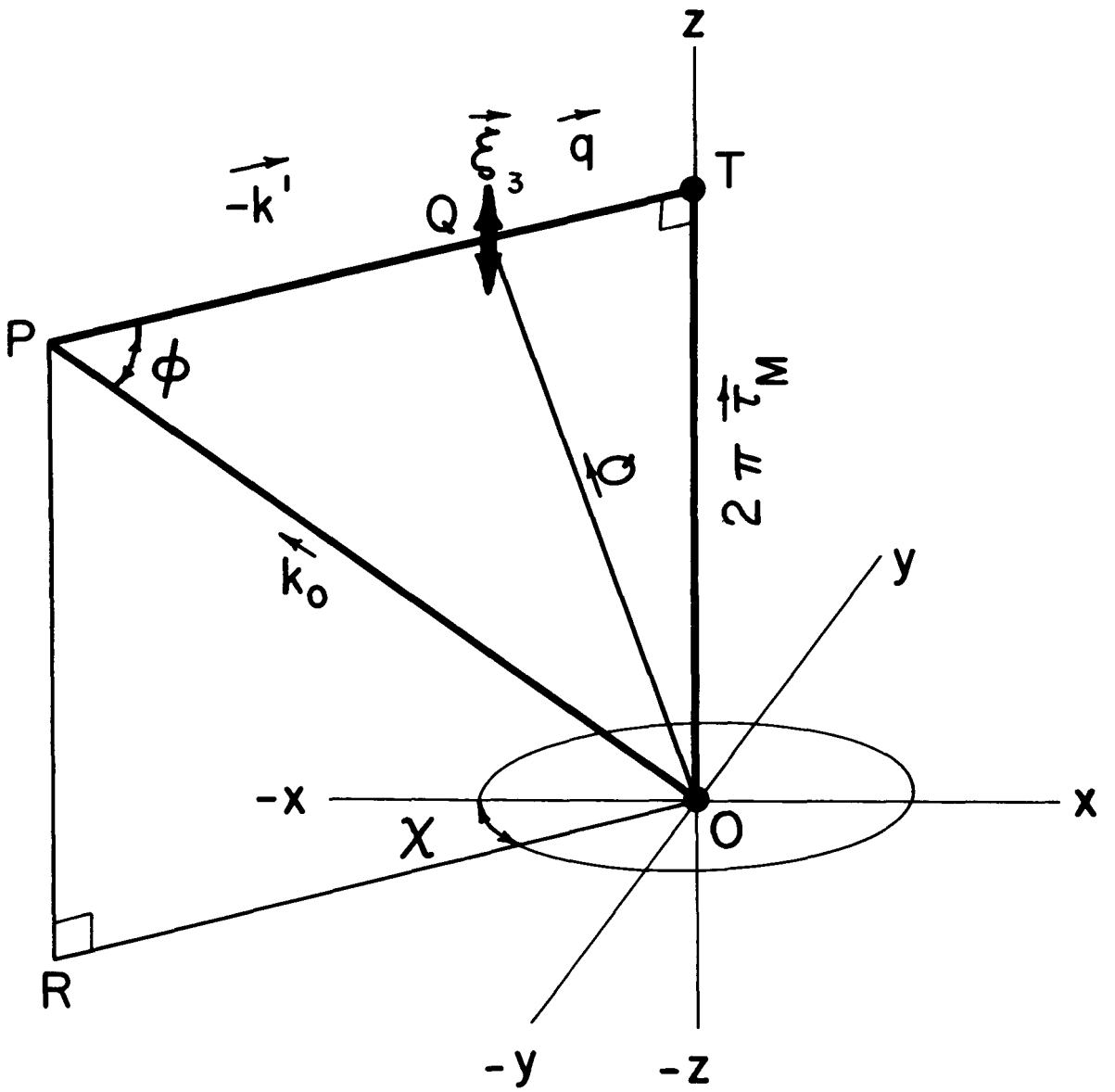

Fig. 2 A vector diagram which illustrates a geometry for studying phonons which have their polarization vector normal to a mirror plane (the x-y plane), as discussed in the text. [§ 2].

A.E.C.L. Ref. # A-2606-G

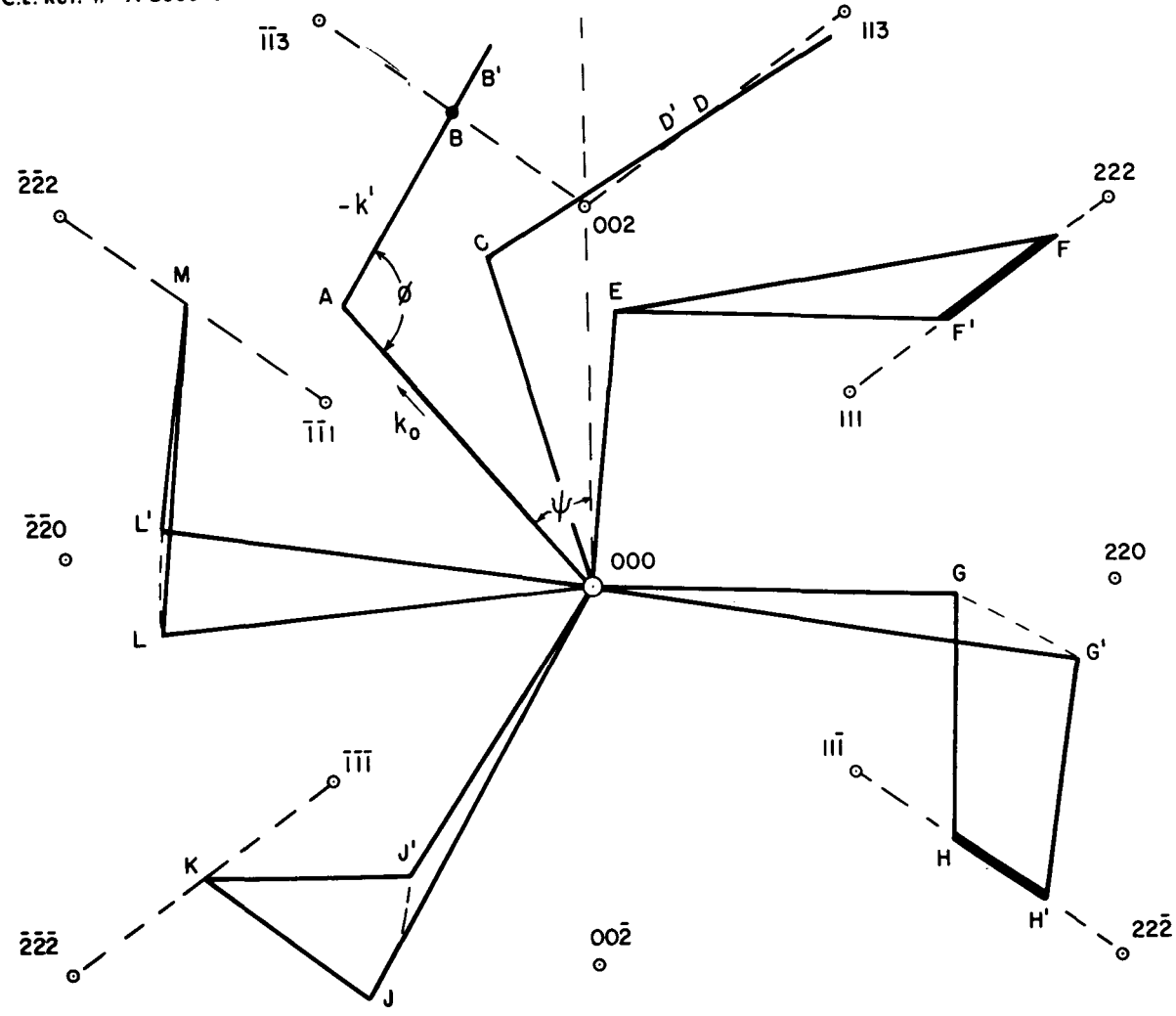

Fig. 3 Vector diagrams which illustrate some of the methods of measuring ν and $\underset{\sim}{q}$ for phonons. Diagram OAB is the conventional method. Diagrams OCD, OEF and OGH represent methods of ensuring that the $\underset{\sim}{q}$ of an observed phonon is in the correct direction. Diagrams OJK and OLM represent the "constant $\underset{\sim}{Q}$" method with variable E_o and E' respectively.

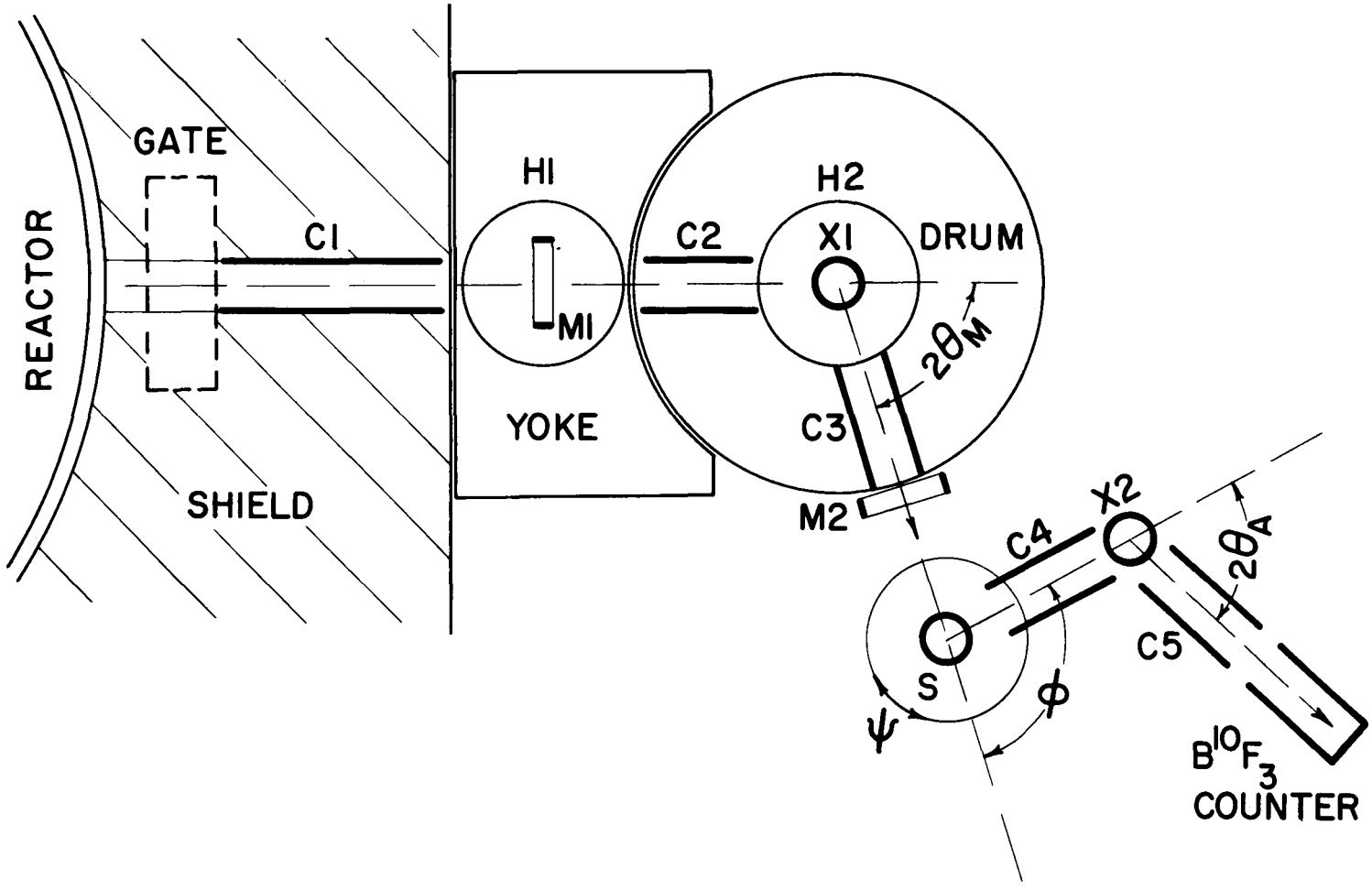

Fig. 4 Schematic diagram of the triple axis crystal spectrometer, showing positions of the collimators C_1 to C_5, the monochromating (X_1) and analyzing (X_2) crystals, the specimen (S), the monitor for the white radiation (M_1) and for the monoenergetic neutrons (M_2). The various independent variables are shown. Facilities H_1 and H_2 are 30 cm. diameter removable sections which can be used in various ways.

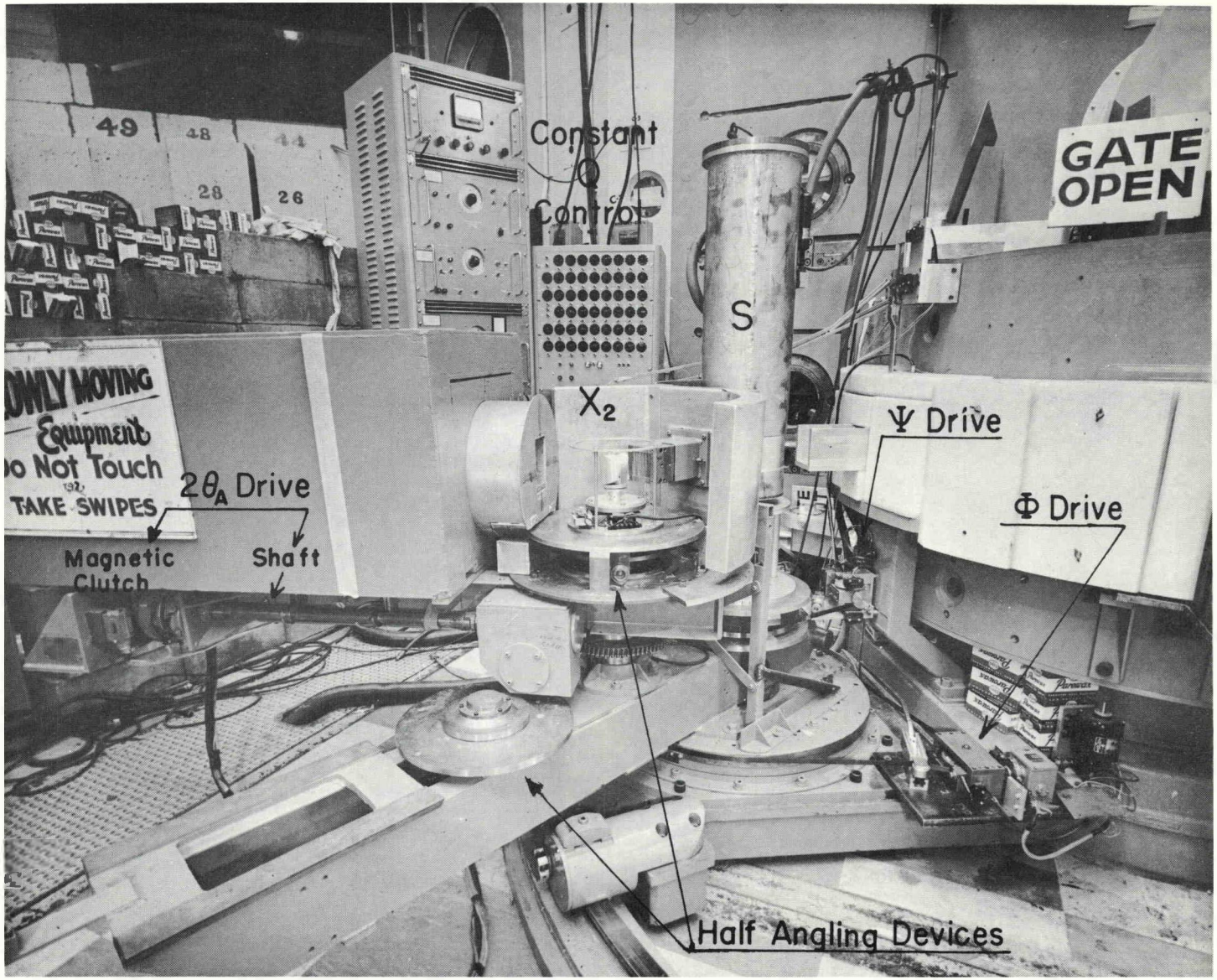

Fig. 5 Photograph of the triple axis spectrometer with labels indicating some components. Some shielding has been removed from the vicinity of the analyzing crystal (X_2).

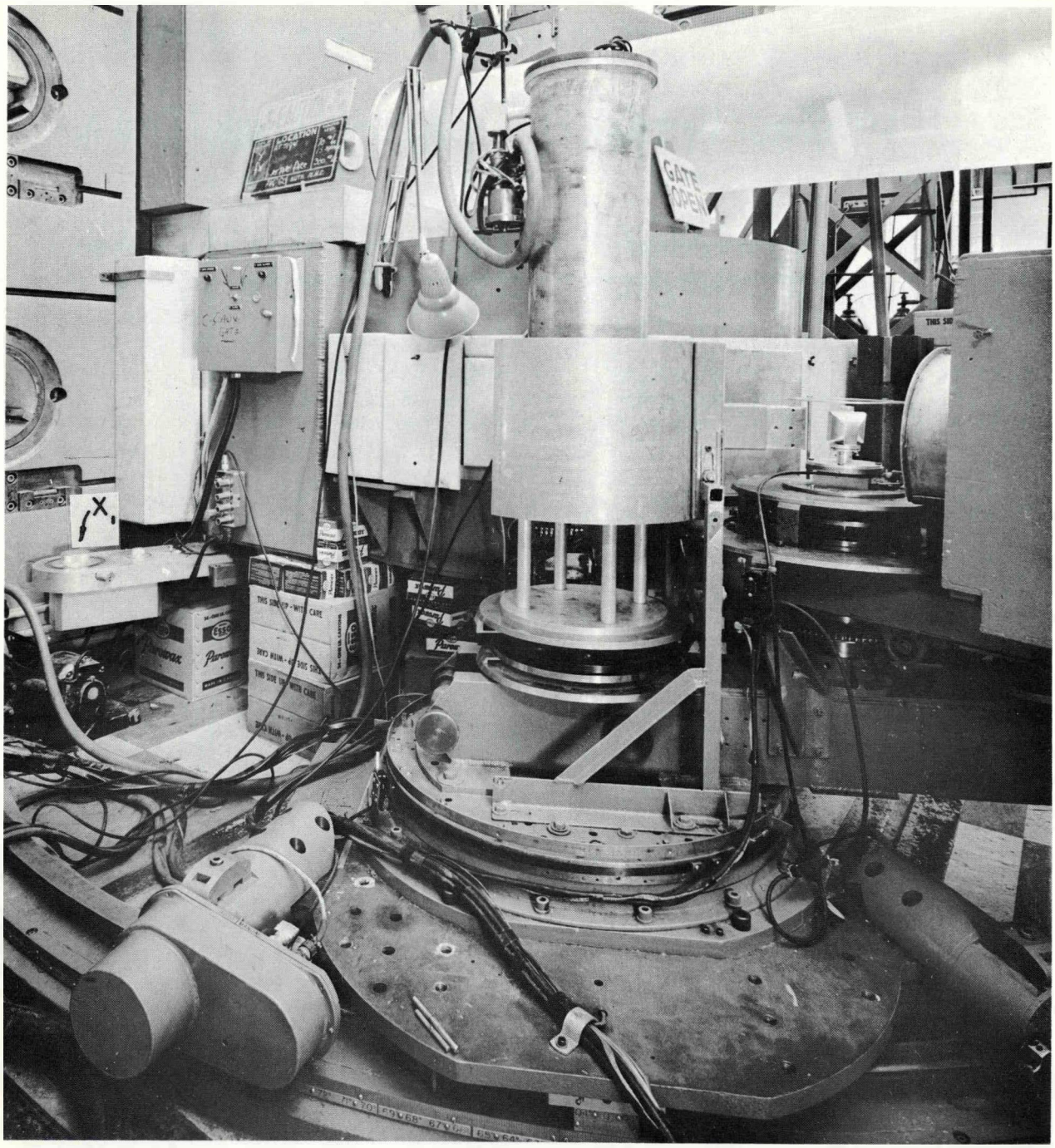

Fig. 6 Another view of the triple axis spectrometer. The control unit for the monochromating crystal X_1 is indicated at the extreme left.

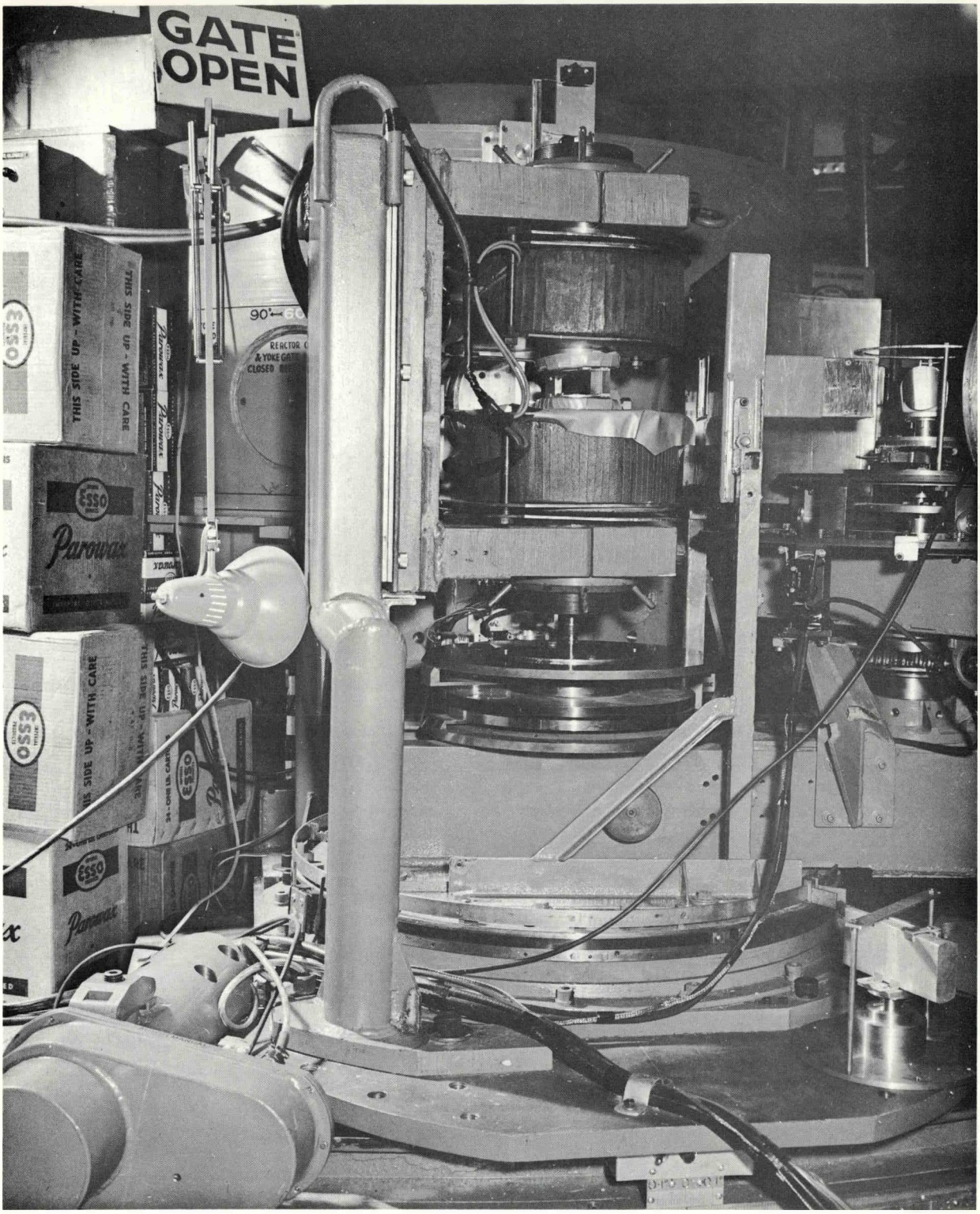

Fig. 7 Another view of the triple axis spectrometer, as set up to measure the dispersion curve of the magnons in F.C.C. cobalt [SINCLAIR et al., ref. (16)]. The cobalt crystal was located between the poles of the magnet and driven from the ψ drive by a shaft through the lower magnet pole. The motor drive for $2\theta_M$ is shown in the lower left hand corner and the vernier for reading $2\theta_M$ at the bottom. Another aluminum analyzer crystal (111 plane, Fankuchen cut) on its plug-in mount is shown in the lower right.

a

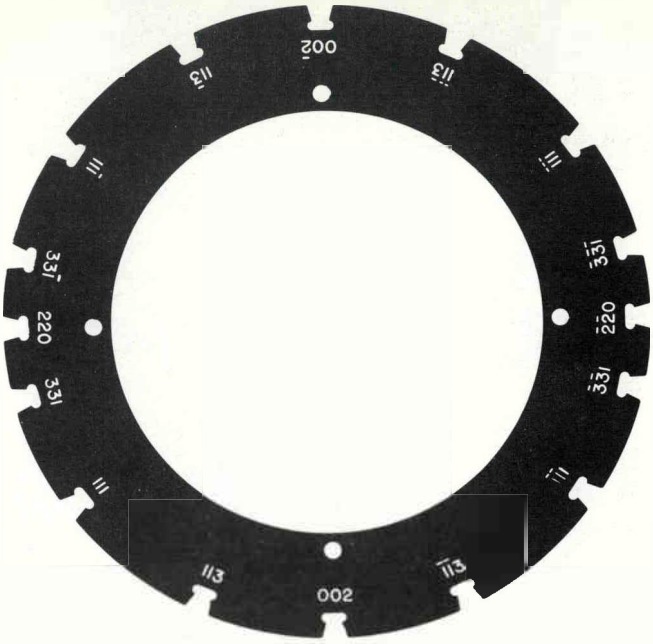

b

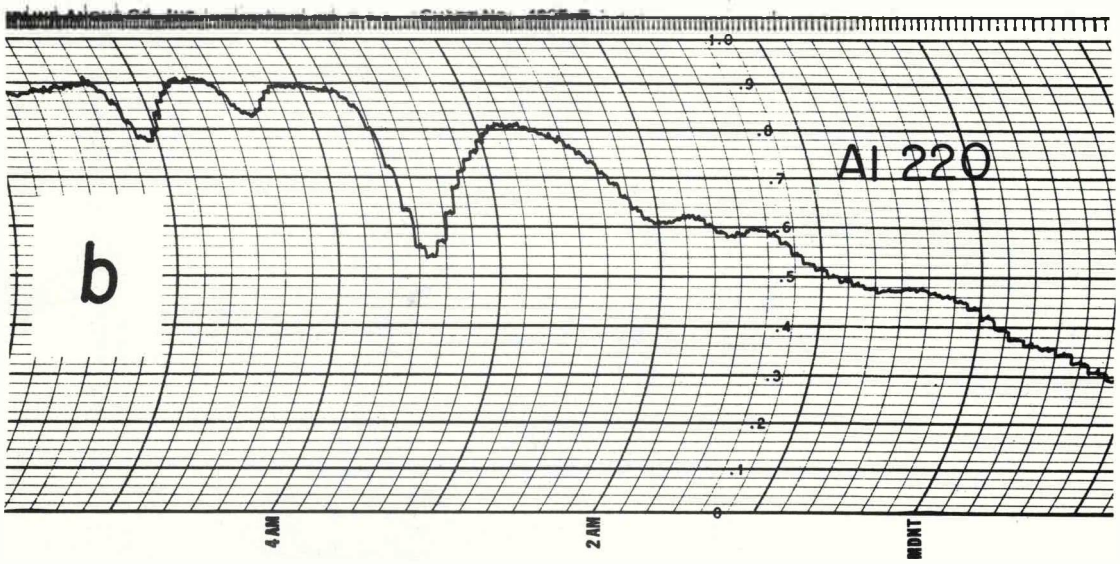

Fig. 8(a) The indexing plate of the monochromating crystal control for the $(1\bar{1}0)$ zone of a face centred cubic monochromator.

(b) A plot of the monitor (M_2) counting rate in the monoenergetic beam with a 220 aluminum monochromator, showing the effects of parisitic reflections. The angular range of $2\theta_M$ shown extends from roughly 35° on the right to 60° on the left and ranges over the peak of the Maxwellian spectrum.

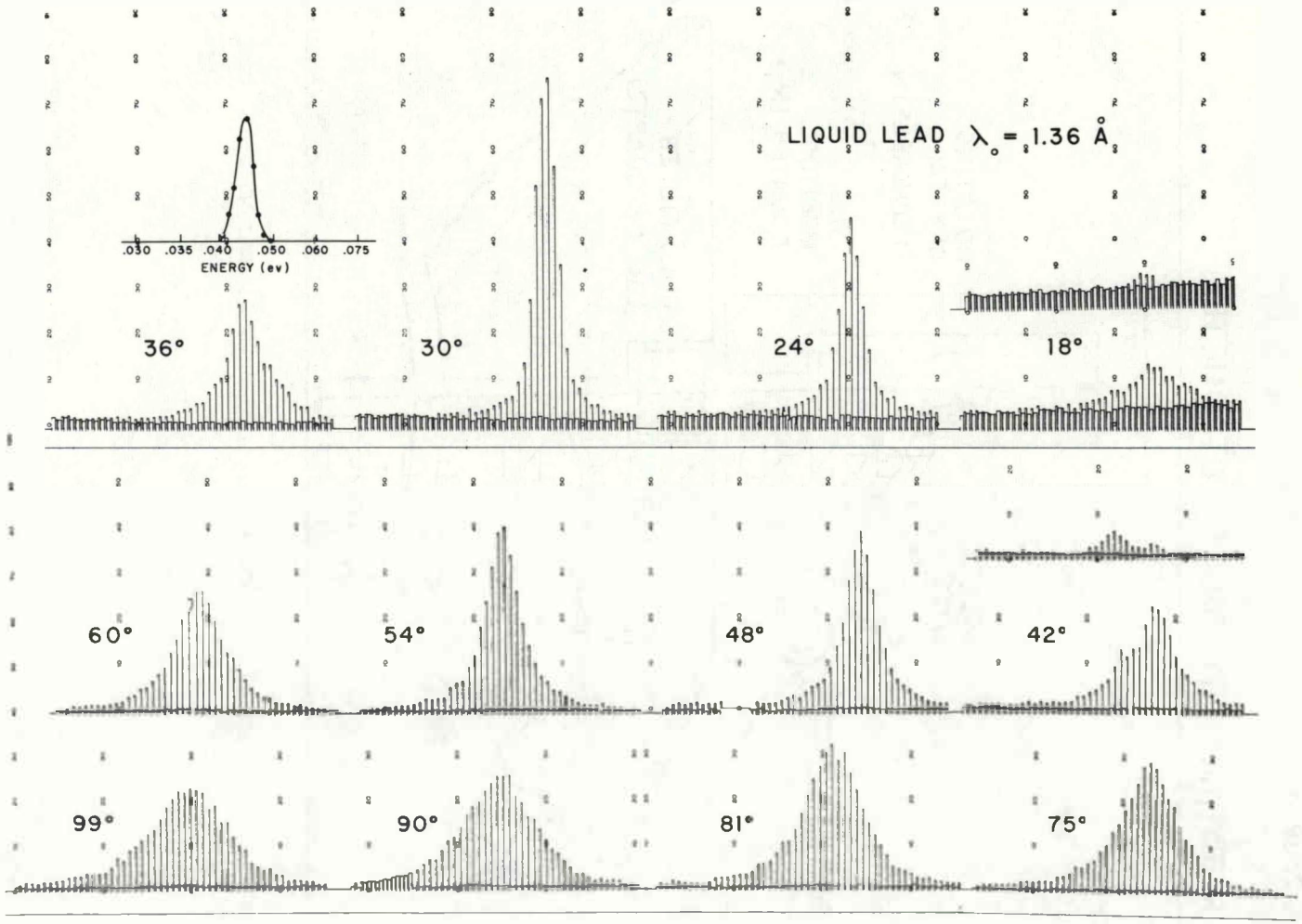

Fig. 9 The distribution of neutrons of initial wavelength 1.36Å scattered by liquid lead [ref. (4)] through various scattering angles, plotted as functions of the analyzing spectrometer angle ($2\theta_A$) in 1/2 degree steps. The distributions were mostly taken in sequence by the spectrometer without attention, and the plots were produced as the experiments progressed by the automatic histogram plotter described in the text. The background with crystal analyzer displaced from the Bragg position was also taken and is shown in the figures. At the top left is shown the resolution function as measured by elastic scattering from vanadium metal, along with an energy scale applicable to all the experiments. At the right are shown two patterns from an empty container, for angles at which the container scattering was especially high.

A.E.C.L. Ref. # A-2539-A

ROTATING CRYSTAL SPECTROMETER

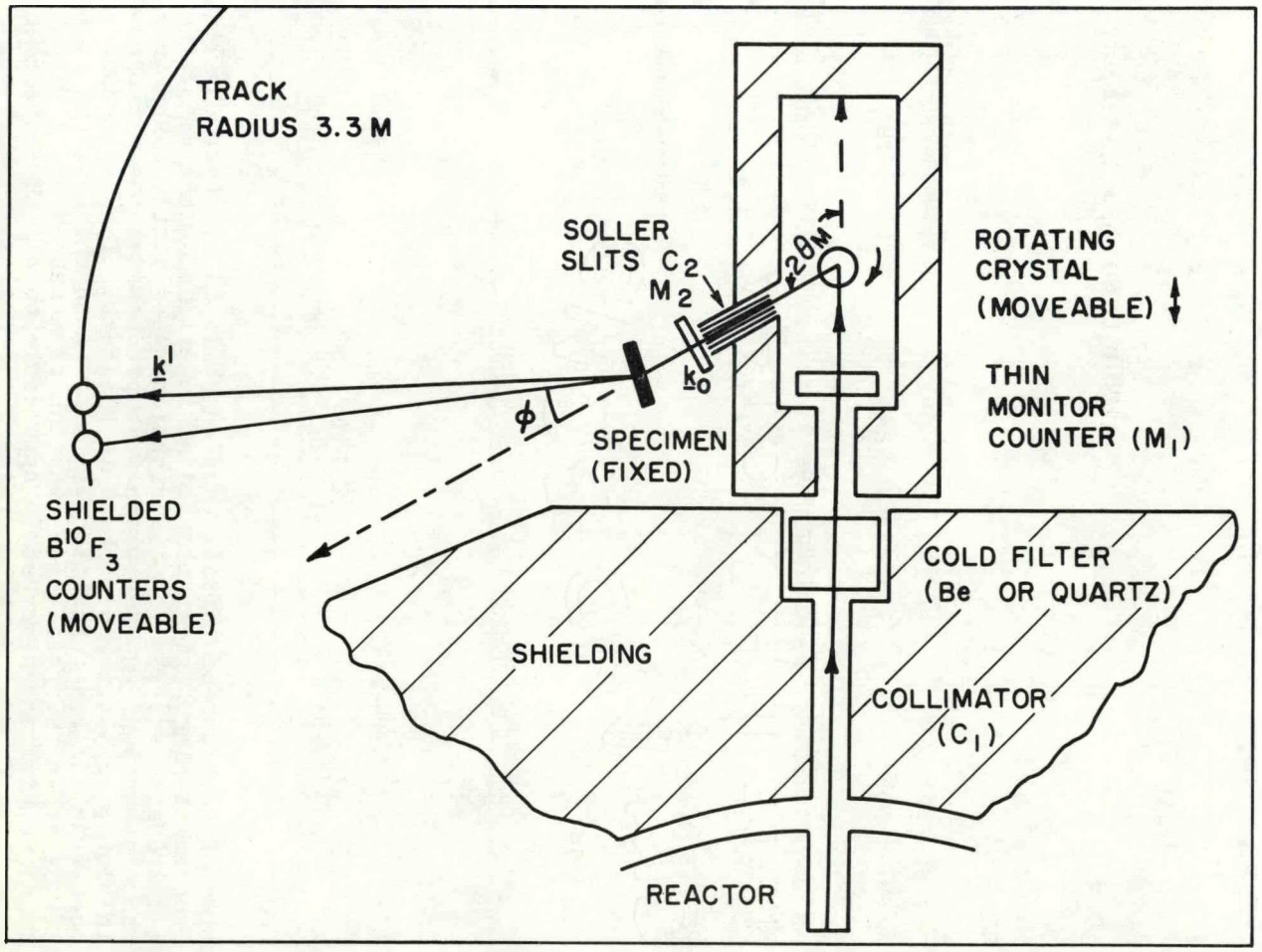

Fig. 10 Schematic diagram of the rotating crystal spectrometer, now at the NRU reactor.

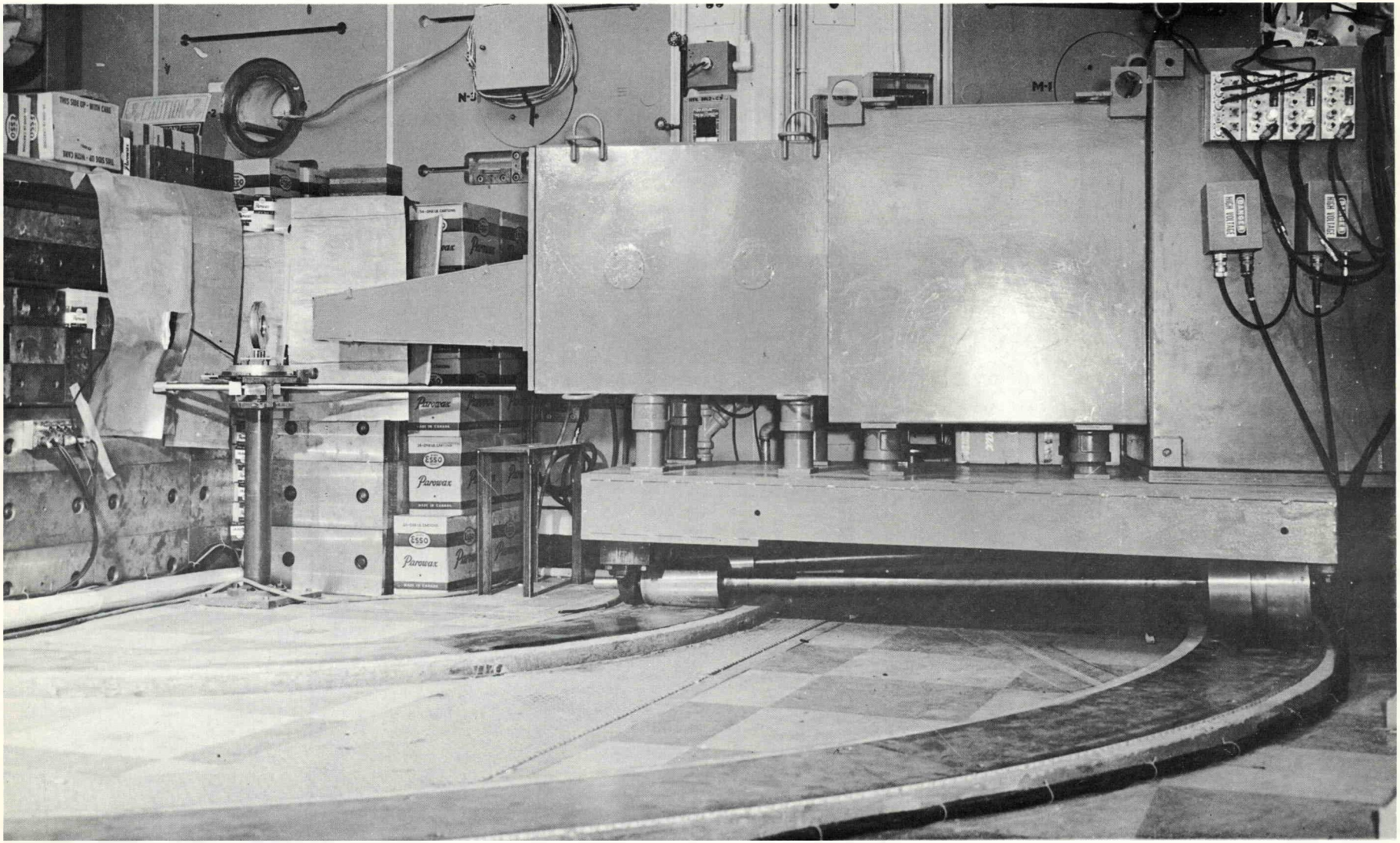

Fig. 11 Photograph of the rotating crystal spectrometer as set up at the NRU reactor. The tapered rollers which keep the platform correctly oriented are easily seen.

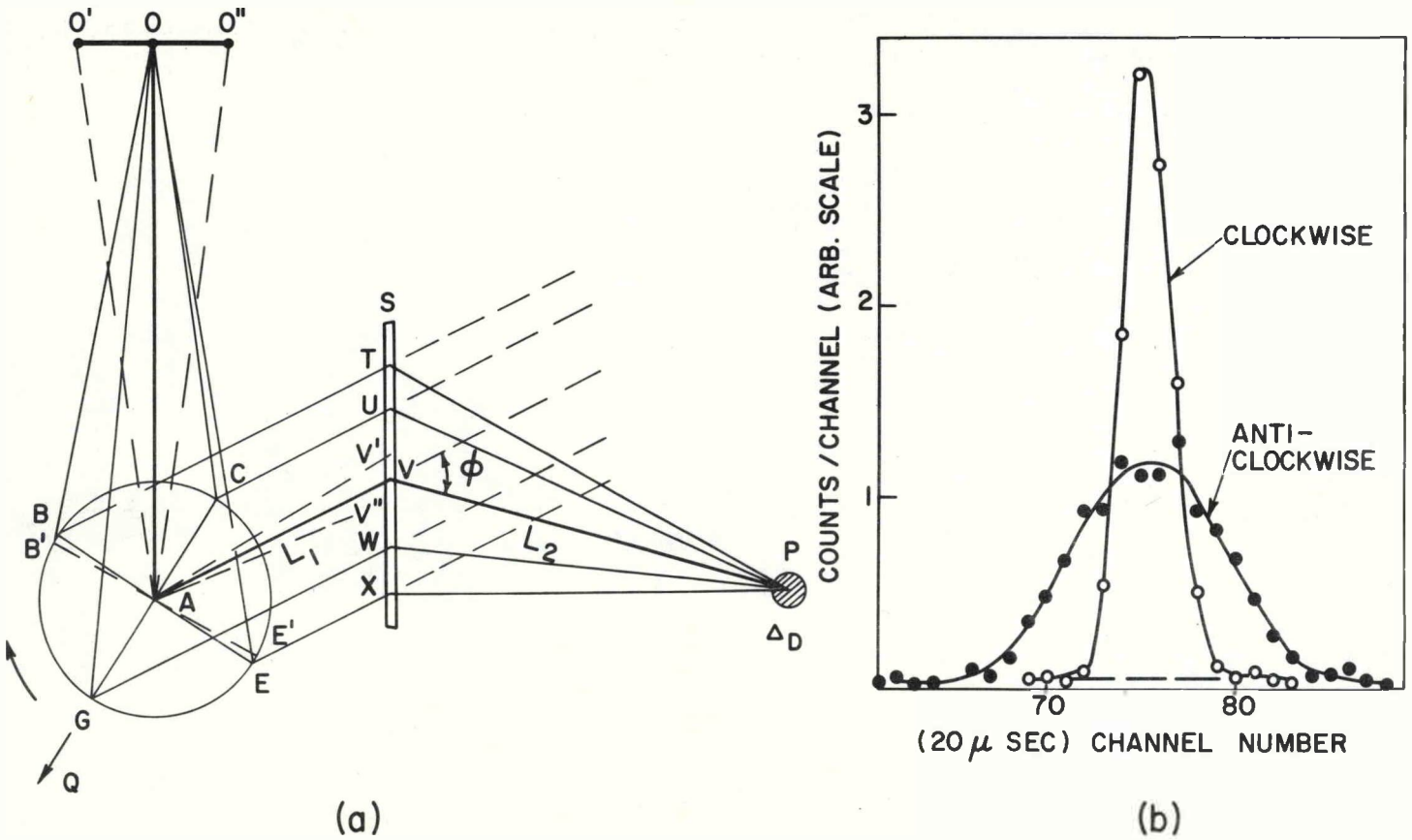

Fig. 12(a) Schematic diagram, much distorted, of the rotating crystal spectrometer, illustrating some of the various paths followed by neutrons. See text.

(b) The elastic scattering by vanadium metal of 4.05Å neutrons with the rotating crystal spinning clockwise and anticlockwise, other conditions being the same. The difference illustrates the importance of the neutron Doppler shift due to the motion of the crystal.

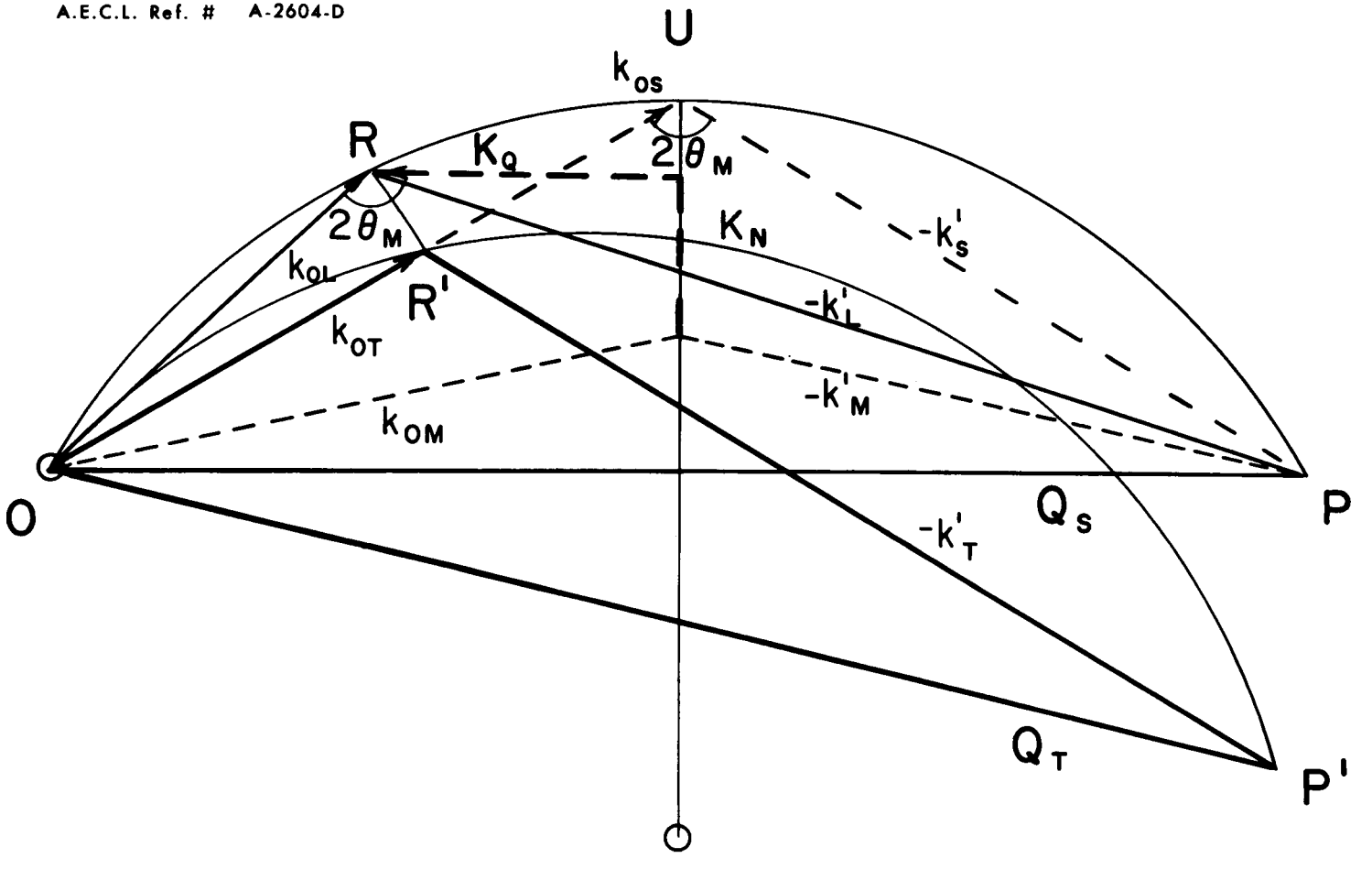

Fig. 13 Reciprocal space diagram for an element of the crystal with a velocity component in the direction of $\underset{\sim}{Q}$ of $\hbar K_Q/m_N$. The vectors $\underset{\sim}{k}_{OS}$ and $-\underset{\sim}{k}'_S$ apply for the crystal stopped. Vectors $\underset{\sim}{k}_O$ and $-\underset{\sim}{k}'$ (laboratory system) satisfy the Bragg condition for the same $\underset{\sim}{Q}$ with the crystal moving. Vectors $\underset{\sim}{k}_{OT}$ and $-\underset{\sim}{k}'_T$ are the wave vectors for the actual burst which occurs with the crystal oriented differently ($\underset{\sim}{Q}_S \rightarrow \underset{\sim}{Q}_T$) than for the crystal stopped.

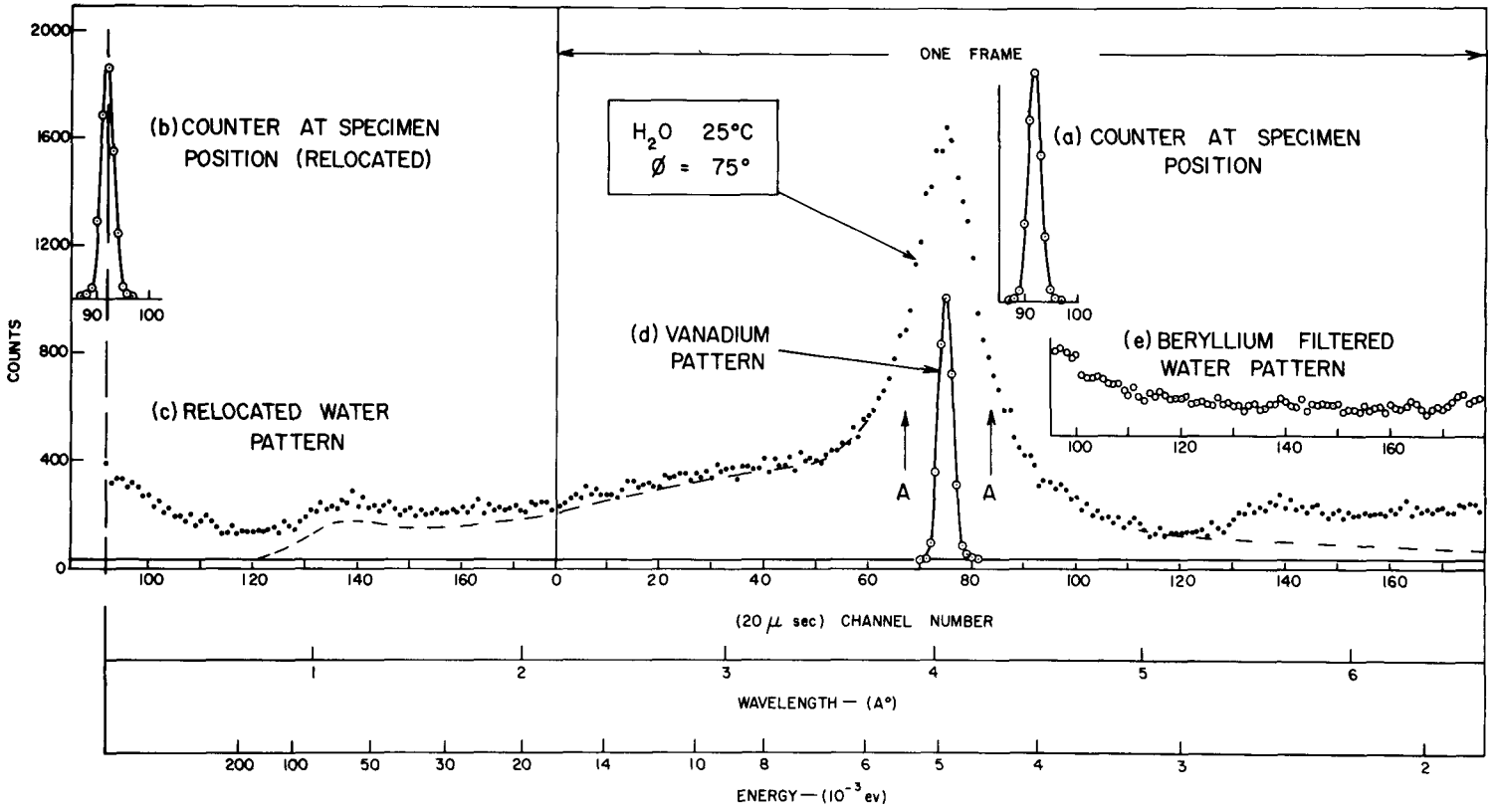

Fig. 14 Time distribution of 4.05Å neutrons scattered by a flat specimen of water at 25°C through an angle of 75° as measured on the rotating crystal spectrometer (25). The transmission of the specimen for 4.05Å neutrons was 78%. The background is shown by the heavy flat line near the abscissa. The distribution for one frame is shown, extended to the left into the preceding frame. Insert (a) shows the distribution obtained with a counter at the specimen position, which gives the zero of the time scale and the resolution function for $E' \to \infty$. Insert (d) shows the elastic scattering from a thin specimen of vanadium which gives the resolution at the incident energy. Insert (e) shows part of the time distribution obtained when a beryllium filter is interposed between the specimen and the counters thus eliminating neutrons with $\lambda < 3.96$Å. The dashed curve shows the distribution for water approximately corrected for frame overlap. The arrows A indicate the supposed positions of the peaks with energy transfer 5×10^{-4} ev reported by HUGHES et al. (26). Only the diffusive broadening (3) is in fact observed.

A.E.C.L. Ref. # A-2627-G

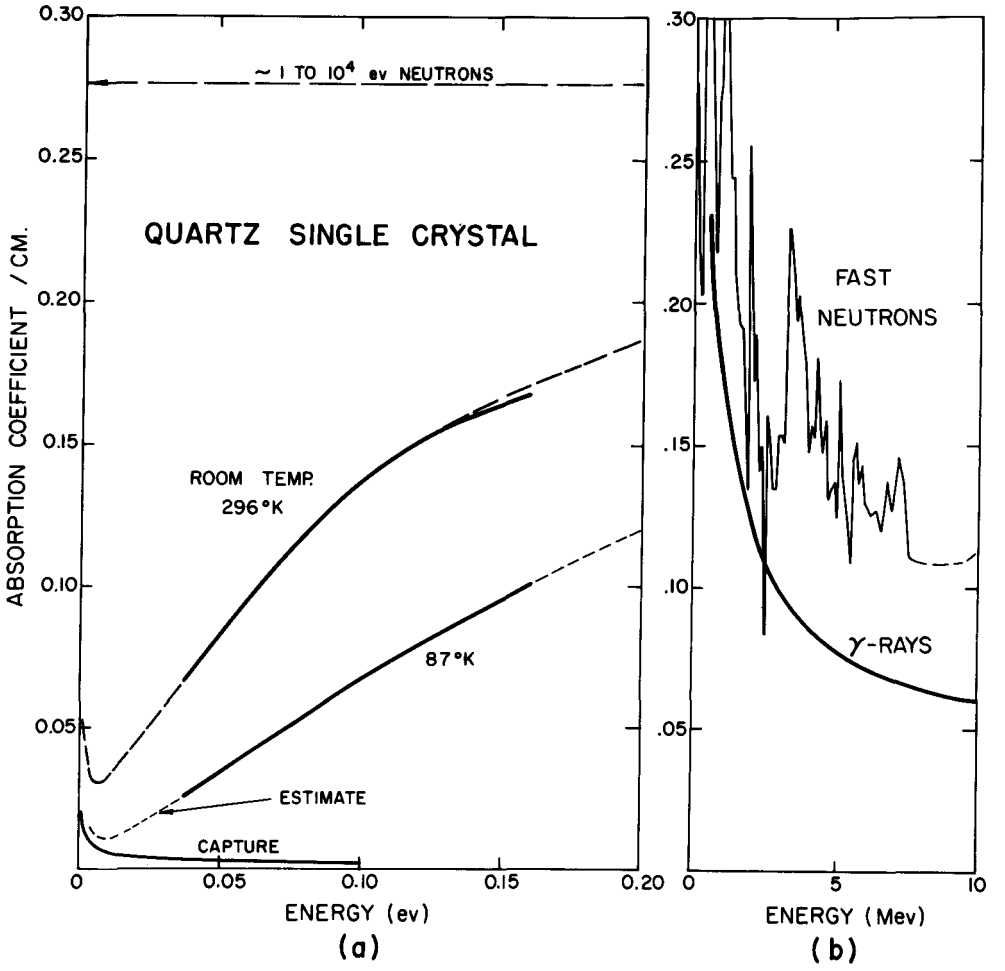

Fig. 15(a) The measured total cross section of a quartz single crystal (per cm length of crystal in units of the cross section of the crystal, i.e. the absorption coefficient), as a function of neutron energy, for temperatures of 296°K and 87°K (solid line). The measurements of RUSTAD et al. (27) for room temperature are shown as a dashed line. An estimate for quartz at 87°K over a more extended energy range, as well as the capture cross section for the silicon in the crystal, are also shown.

(b) Similar cross sections for fast neutrons and γ-rays, as computed from data in refs. (28) and (29).